Research article

JHEP|Reports

Altered fatty acid metabolism rewires cholangiocarcinoma stemness features

Giulia Lori[1], Mirella Pastore[1], Nadia Navari[1], Benedetta Piombanti[1], Richell Booijink[2], Elisabetta Rovida[3], Ignazia Tusa[3], Monika Lewinska[4], Jesper B. Andersen[4], Tiziano Lottini[1], Annarosa Arcangeli[1], Maria Letizia Taddei[1], Erica Pranzini[3], Caterina Mancini[1], Cecilia Anceschi[3], Stefania Madiai[1], Elena Sacco[5], Stefano Rota[5], Adriana Trapani[6], Gennaro Agrimi[7], Matteo Ramazzotti[3], Paola Ostano[8], Caterina Peraldo Neia[8], Matteo Parri[3], Fabrizia Carli[9], Silvia Sabatini[9], Amalia Gastaldelli[9], Fabio Marra[1,*,†], Chiara Raggi[1,*,†]

JHEP Reports **2024**. vol. 6 | 1–14

Background & Aims: Among the reprogrammed metabolic pathways described in cancer stem cells, aberrant lipid metabolism has recently drawn increasing attention. Our study explored the contribution of fatty acids (FA) in the regulation of stem-like features in intrahepatic cholangiocarcinoma (iCCA).

Methods: We previously identified a functional stem-like subset in human iCCA by using a three-dimensional sphere (SPH) model in comparison to parental cells grown as monolayers (MON). In this study, quantification of intracellular free FA and lipidomic analysis (triacylglycerol [TAG] composition, *de novo* synthesis products) was performed by Liquid chromatography–mass spectrometry (LC–MS); quadrupole time-of-flight liquid chromatography/mass spectrometry (Q-TOF LC/MS), respectively, in both SPH and MON cultures.

Results: Stem-like SPH showed a superior content of free FA (citric, palmitic, stearic, and oleic acids) and unsaturated TAG. Molecularly, SPH showed upregulation of key metabolic enzymes involved in *de novo* FA biosynthesis (AceCS1, ACLY, ACAC, FASN, ACSL1) and the mTOR signalling pathway. In patients with iCCA (n = 68), tissue expression of *FASN*, a key gene involved in FA synthesis, correlated with 5-year overall survival. Interference with FASN activity in SPH cells through both specific gene silencing (siRNA) or pharmacological inhibition (orlistat) decreased sphere-forming ability and expression of stem-like markers. In a murine xenograft model obtained by injection of iCCA-SPH cells, FASN inhibition by orlistat or injection of *FASN*-silenced cells significantly reduced tumour growth and expression of stem-like genes.

Conclusion: Altered FA metabolism contributes to the maintenance of a stem-like phenotype in iCCA. FASN inhibition may represent a new approach to interfere with the progression of this deadly disease.

Introduction

Stem cell programs in cancer initiation, progression, and therapy resistance are considered the centrepiece of tumour biology. The identification of cancer stem cells (CSC) in many solid tumours, including hepatic cancer,[1–3] has provided novel insights into the mechanisms of carcinogenesis. In cholangiocarcinoma (CCA), the presence of stem-like cells has been correlated with more aggressive tumour characteristics and poorer patient prognosis.[4] Investigation on CSC has been favoured by the development of *in vitro* systems enriched in stem-like cells. In this regard, we and others have developed and adopted three-dimensional (3D) tumour sphere (SPH) formation as an efficient *in vitro* tool to enrich stem-like cells.[1–3]

Although studies on CSC biology have identified relevant signals sustaining tumour stemness, the exploration of metabolic reprogramming in the control of the stem state is in its infancy. Novel lines of evidence are shedding light on the dependence of CSC on lipid metabolism and particularly on fatty acids (FA).[5–8] This emerging concept linking lipid metabolism and stem cell fate mostly derives from studies assigning a CSC-promoting function to the excess of monounsaturated FA.[9,10]

Recently, new experimental evidence, although divergent, has highlighted a role for lipid metabolism in the pathogenesis of CCA. In line with the histological and molecular heterogeneity of this neoplasm, highly proliferative CCA cells are strongly lipid-dependent, as shown by their upregulated lipid and lipoprotein uptake and catabolism. Conversely, more advanced stages of disease or CCAs associated with *Clonorchis sinensis* infection exhibit elevated expression of *FASN*. Furthermore, in lymph node metastases, CCA colonisation appears to be driven by PPARγ-regulated lipid metabolic reprogramming.[11–15]

* Corresponding authors. Addresses: Department of Experimental and Clinical Medicine, University of Florence, Cubo Centro Polivalente 2, Viale Pieraccini, 6, I50134 Florence, Italy. Tel.: +39 0552758128 (C. Raggi); Department of Experimental and Clinical Medicine, University of Florence, Largo Brambilla, 3I50134 Florence, Italy. Tel.: +39 0557945425 (F. Marra).
E-mail addresses: chiara.raggi@unifi.it (C. Raggi), fabio.marra@unifi.it (F. Marra).
† These authors are co-senior authors.
https://doi.org/10.1016/j.jhepr.2024.101182

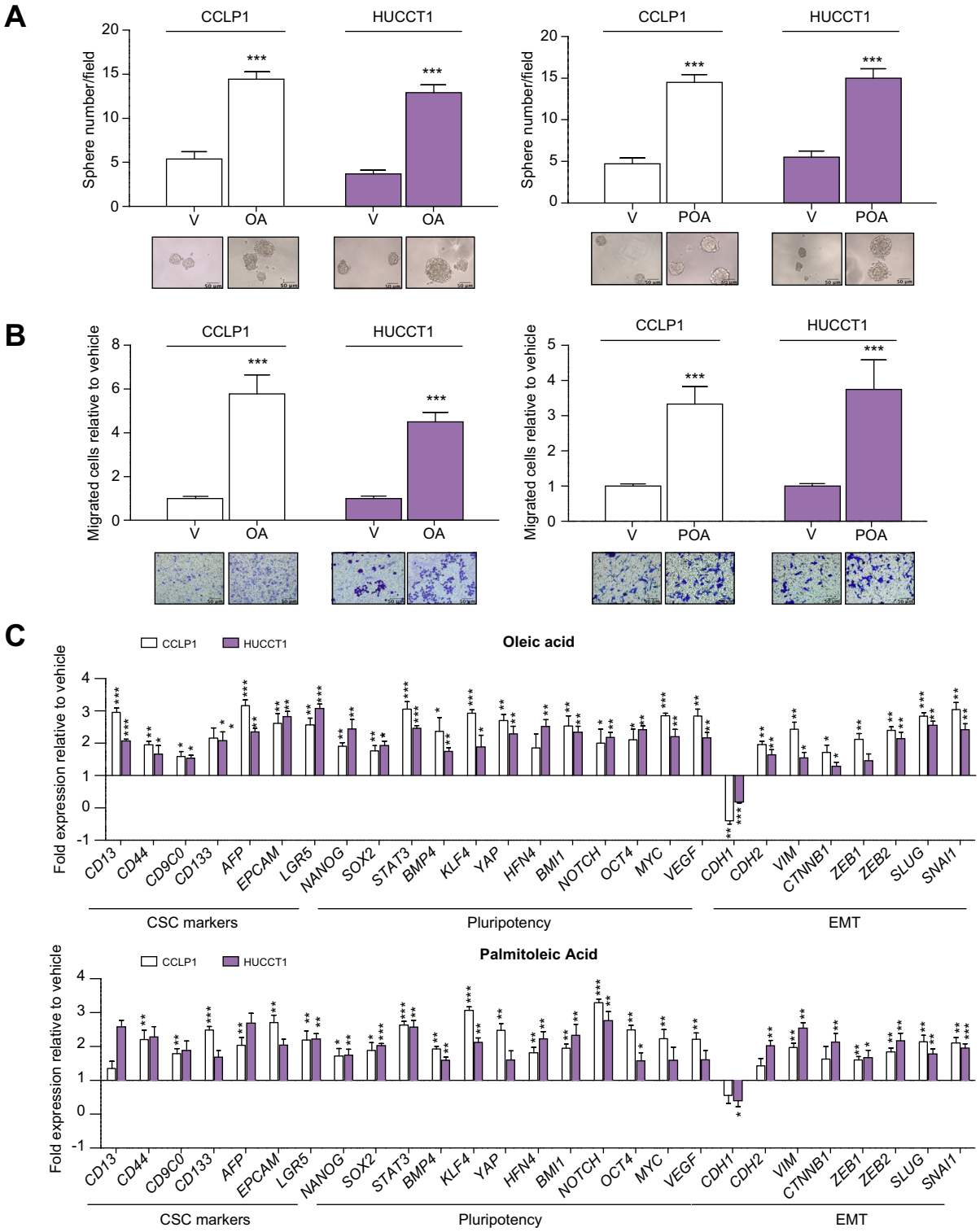

Fig. 1. Effects of monounsaturated FAs on stem-like proprieties in iCCA cells. (A) iCCA cells were grown as spheres for 7 days, in presence or absence of FAs. Then SPH were counted, and their volume was measured. Mean ± SEM (n = 3, ***p ≤0.001). Representative images of iCCA SPH are reported below the graphs (original magnification 40×). (B) Migration of iCCA cells was measured in modified Boyden chambers, after 48 h treatment. Mean ± SEM (n = 3, ***p ≤0.001). Representative images of the filters are shown below the barograms (original magnification 40×, scale bar 10 μM). (C) Expression of different genes involved in EMT, drug-resistance and stem-like acquisition in CCLP1 and HUCCT1 cells were treated with OA or POA for 48 h, reported as fold changes normalised to mean expression of vehicle-treated cells. Mean ± SEM (n = 3, *p ≤0.05, **p ≤0.01, ***p ≤0.001; Mann–Whitney U test). EMT, epithelial to mesenchymal transition; FA, fatty acids; iCCA, intrahepatic cholangiocarcinoma; SPH, sphere cultures; OA, oleaic acid; POA, palmitoleic acid; V, vehicle.

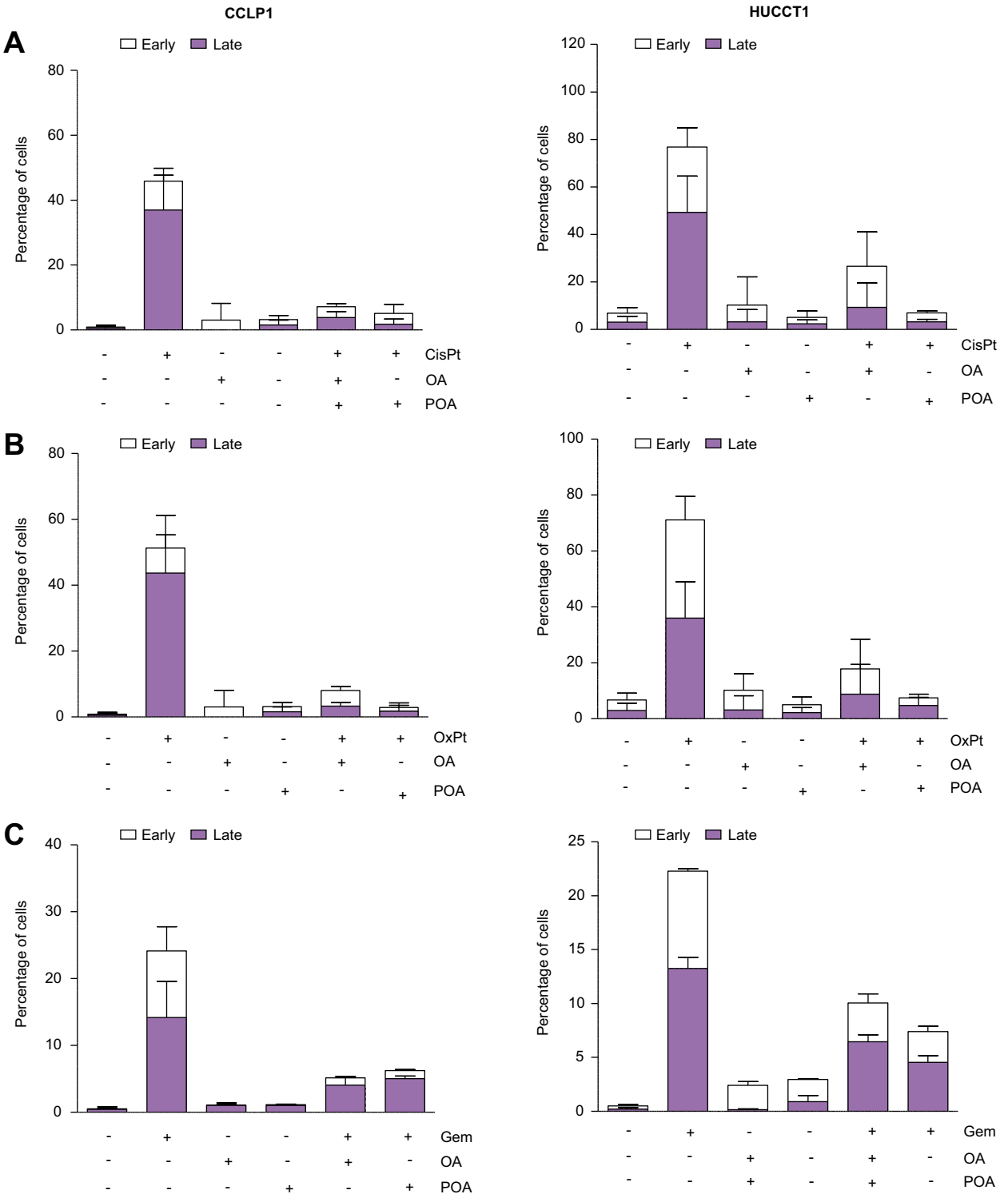

Fig. 2. Monounsaturated FAs pretreatment protects iCCA cells from antiblastic toxic effects. CCLP1 and HUCCT1 cells were pretreated for 24 h with oleic acid (OA) or palmitoleic acid (POA) in starvation medium, then with (A) cisplatin, (B) oxaliplatin, or (C) gemcitabine for a further 24 h. Apoptosis was measured with Annexin V/PI staining. Data are presented as mean ± SEM (n = 3). Complete statistical data are shown in Table S3; FA, fatty acids; iCCA, intrahepatic cholangiocarcinoma; OA, oleic acid; POA, palmitoleic acid; CisPt, cisplatin; OxPt, oxaliplatin; Gem, gemcitabine.

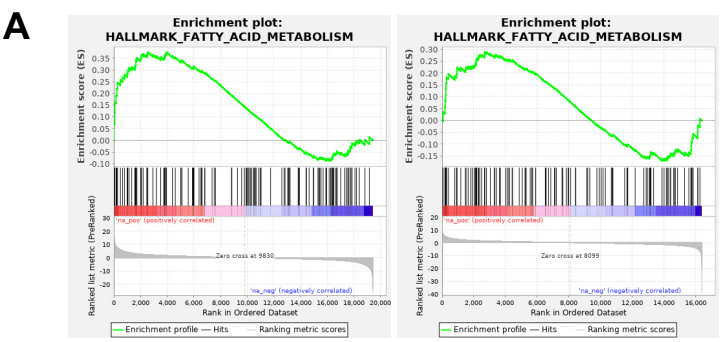

	ES	NES	FDR q-VAL
CCLP1 SPH	0.288	1.153	0.285
HUCCT1 SPH	0.376	1.393	0.042

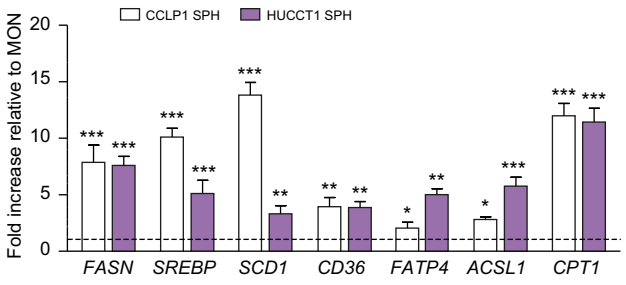

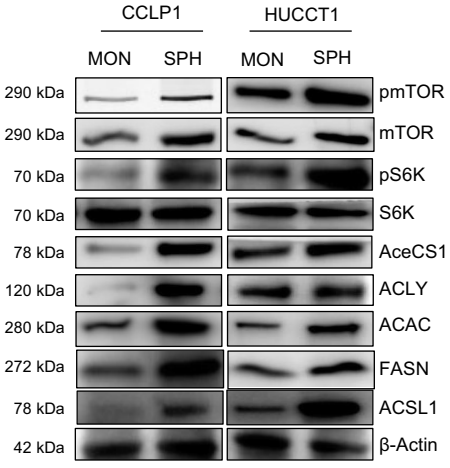

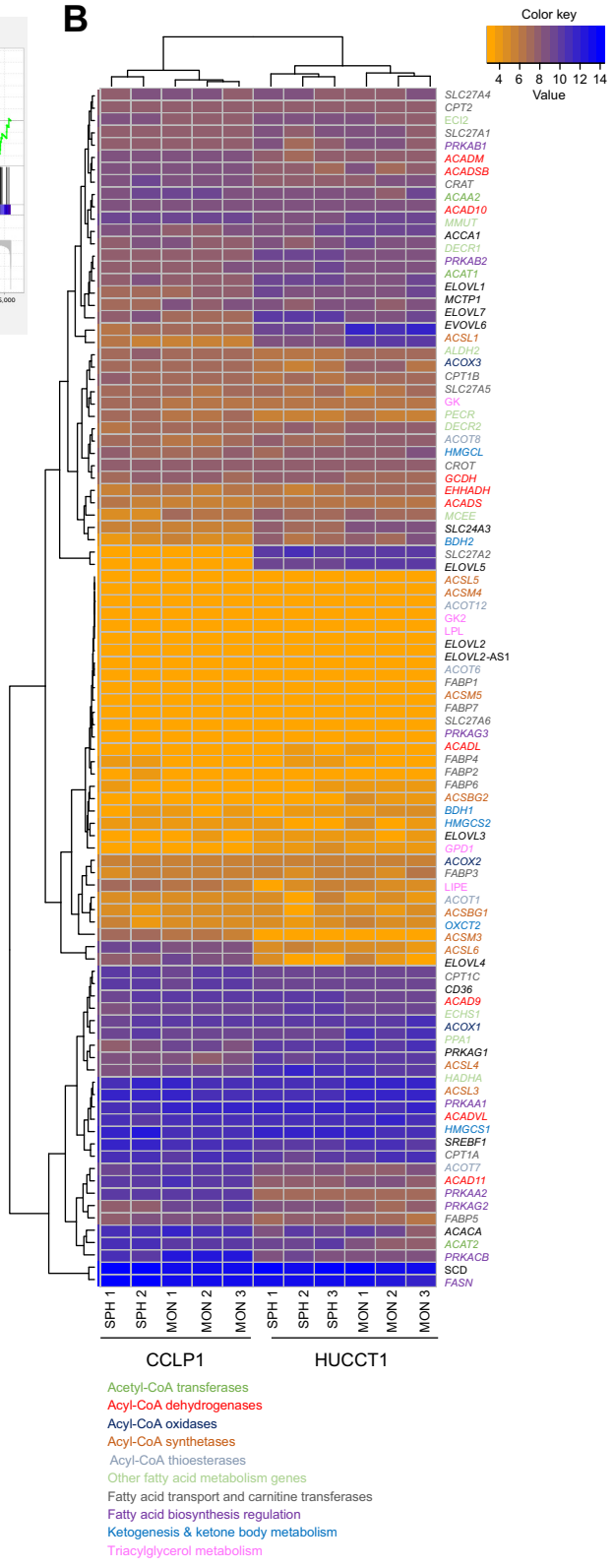

Fig. 3. Molecular aspects behind altered FA pathways in iCCA stem-like cells. (A) Results of a GSEA Pre-ranked analysis on the fatty acids metabolism gene set of the Hallmark MSigDB collection. (B) Heatmap plot of differentially expressed genes of the genes involved in fatty acid metabolism in SPH and MON, using Euclidean distance as similarity metrics and complete linkage as linkage method. Modified Z-scores of the individual genes, as median-centred $\log_2$ intensity values divided by standard deviation, are shown by a blue-to-red gradient variation. Different colours specified different FA metabolic pathways. (C) CCLP1 and HUCCT1 cells were grown as MON) or as SPH, then RNA was extracted. Expression of different genes involved in FA metabolism is reported as fold changes normalised to mean expression of MON. Mean ± SEM (n = 3, *p ≤0.05, ** p ≤0.01, *** p ≤0.001; Mann–Whitney U test). (D) Representative immunoblot of mTOR, phospho-mTOR, S6K,

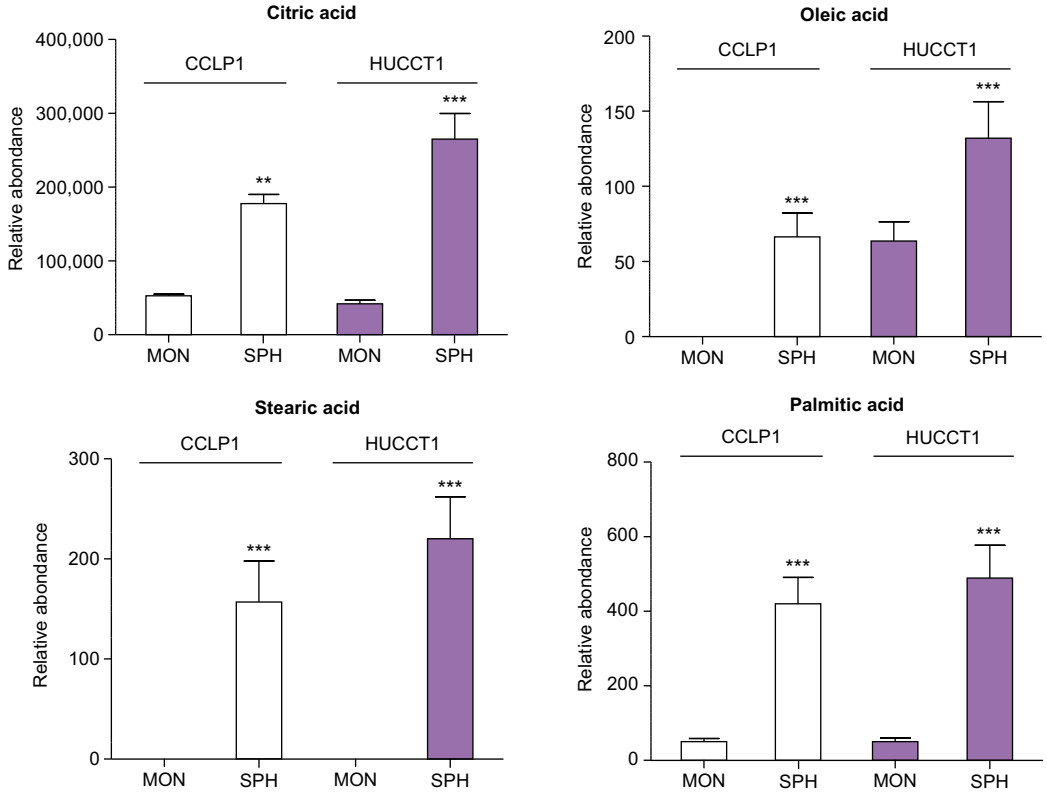

Fig. 4. Content of free FA in iCCA stem-like compartment. Relative metabolite abundance of intracellular free citric, stearic, oleic, and palmitic acid in CCLP1 or HUCCT1 cell lines, grown in MON or as SPH, identified by LC-MS analysis. Peak areas obtained were normalised for protein content for each sample. Mean ± SEM (n = 9, $^{**}p \leq 0.01$, $^{***}p \leq 0.001$; Mann–Whitney *U* test). FA, fatty acids; iCCA, intrahepatic cholangiocarcinoma; MON, monolayer; SPH, sphere cultures.

Despite these recent lines of evidence, little is known about the role of lipids and lipid metabolism in iCCA-stemness. Here we show that altered FA metabolism is a distinctive feature of tumour stem-like cells in iCCA.

Materials and methods

Extraction of metabolites

For the monolayer (MON) cell culture, cells cultured in a six well-plate were quickly rinsed with NaCl 0.9% and quenched with 500 μl ice-cold 70:30 acetonitrile:water. Plates were placed at -80 °C for 10 min, then cells were collected by scraping and sonicated 5 s for five pulses at 70% power twice. For the SPH cell culture, 48 spheroids were collected from each well of a 96-well plate and centrifuged at 600 rpm for 5 min at 4 °C. Pellets were washed with 1 ml of NaCl 0.9%, centrifuged as above, and resuspended in 500 μl ice-cold 70:30 acetonitrile:water. Samples were placed at -80 °C for 10 min and then sonicated 5 s for five pulses at 70% power twice. At this point, for both MON and SPH experiments, samples were centrifuged at 12,000 × *g* for 10 min and supernatants were collected using a glass insert and dried in a centrifugal vacuum concentrator (Concentrator plus/Vacufuge plus, Eppendorf) at 30 °C for about 2.5 h. Samples were then resuspended with 150 μl H_2O prior to analyses.

Liquid chromatography-mass spectrometry analysis

Liquid chromatography (LC) separation was performed using an Agilent 1290 Infinity UHPLC system and an InfintyLab Poroshell 120 PFP column (2.1 × 100 mm, 2.7 μm; Agilent Technologies). Mobile phase A was water with 0.1% formic acid. Mobile phase B was acetonitrile with 0.1% formic acid. The injection volume was 10 μl and LC gradient conditions were: 0 min: 100% A; 2 min: 100% A; 4 min: 99% A; 10 min: 98% A; 11 min: 70% A; 15 min: 70% A; and 16 min: 100% A with 2 min of post-run. The flow rate was 0.2 ml/min and the column temperature was 35 °C. MS detection was performed using an Agilent 6550 iFunnel Q-TOF mass spectrometer with Dual JetStream source operating in negative ionisation mode. MS parameters were: gas temperature: 285 °C; gas flow: 14 L/min; nebuliser pressure: 45 psig; sheath gas temperature: 330 °C; sheath gas flow: 12 L/min; VCap: 3,700 V; Fragmentor: 175 V; Skimmer: 65 V; and Octopole RF: 750 V. Active reference mass correction was done through a second nebuliser using masses with m/z: 112.9855 and 1,033.9881. Data were

phosphoS6K, AceCS1, ACLY, ACAC, FASN, ACSL1 protein levels in CCLP1 and HUCCT1 cells grown as MON and SPH. β-Actin immunoblot was performed to ensure equal loading. ES, enrichment score; FA, Fatty Acids; FDR, false discovery rate; GSEA, gene set enrichment analysis; MFI, mean fluorescent intensity; NES, normalised enrichment score; iCCA, intrahepatic cholangiocarcinoma; MON, monolayer; SPH, sphere cultures.

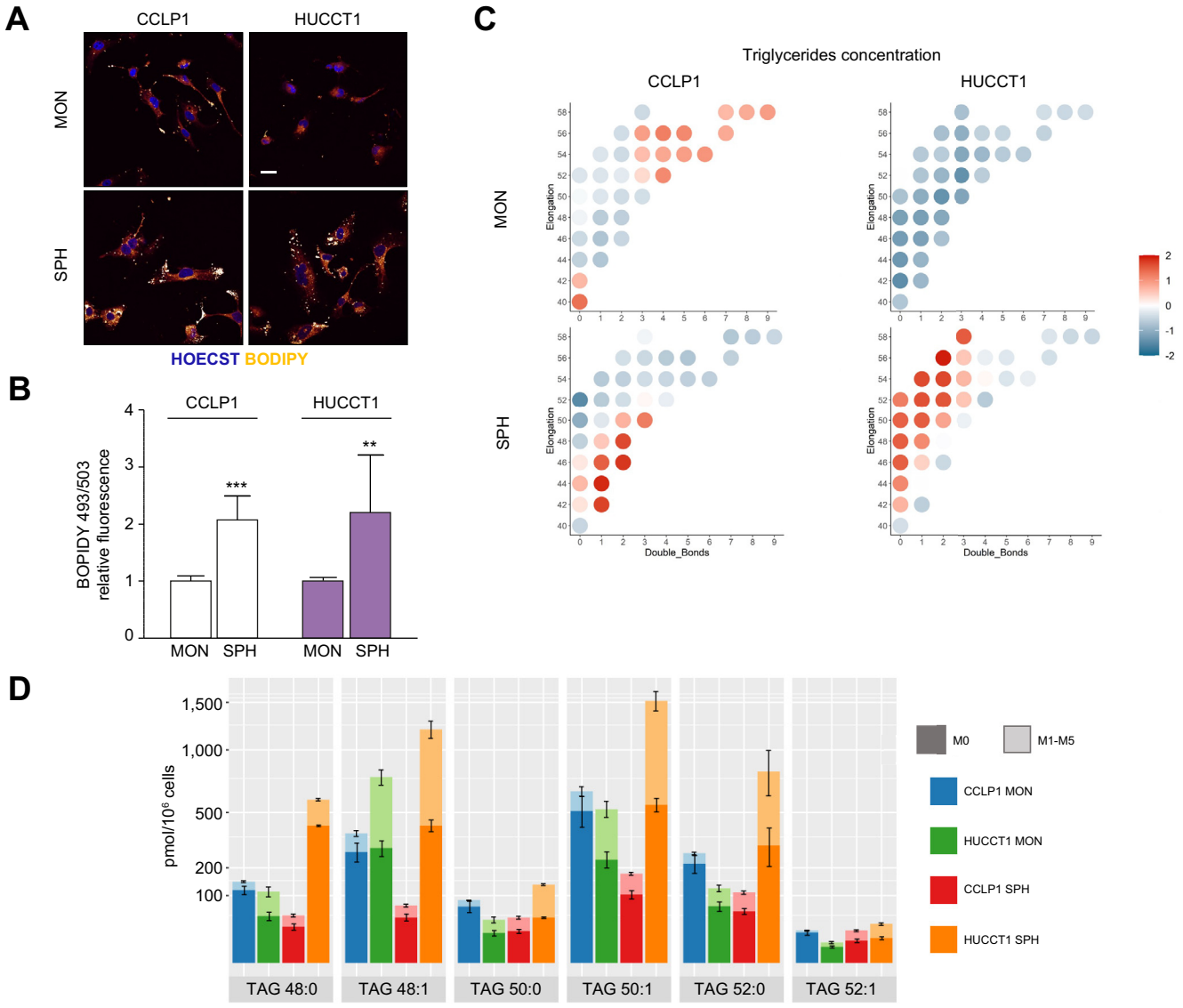

	% *de novo* synthesized TG *p <0.05 MON *vs.* SPH					
	TAG 48:0	TAG 48:1	TAG 50:0	TAG 50:1	TAG 52:0	TAG 52:1
CCLP1 MON	20%*	27%*	20%*	21%*	13%*	19%*
CCLP1 SPH	56%	62%	51%	55%	38%	42%
HUCCT1 MON	43%*	37%*	52%*	41%*	53%*	47%*
HUCCT1 SPH	67%	65%	67%	63%	59%	62%

Fig. 5. Triglyceride composition in iCCA cells grown as monolayers or spheres. (A) Intrahepatic CCA cells were grown as MON or SPH, then cells were stained with Bodipy 493/503. Confocal microscopy analysis of lipid droplets in MON and SPH. (light yellow: Bodipy 493/503; blue: Hoechst; scale bar = 5 μm). (B) Lipid droplets quantification by cytofluorimetric analysis. Histograms represent the MFI of the Bodipy probe normalised to mean MFI of MON. Results are mean ± SEM (n = 3, **p ≤0.01, ***p ≤0.001; Mann–Whitney *U* test). (C) Representation of triglycerides concentration in CCLP1 and HUCCT1 grown as MON or SPH, respectively. Single triglycerides were identified according to their degree of saturation (x axis) *i.e.,* the number of double bonds, and elongation number (y axis) *i.e.,* the number of carbons. Triglycerides concentrations were scaled to zero mean and unit variance and reported as median for each cell line grown as MON or SPH. (D) Concentration of the main saturated TAG and their desaturated counterparts in CCLP1 MON (blue), SPH (green), HUCCT1 MON (red), SPH (orange) cultured cells, respectively. The measured concentrations are composed by two parts: the *de novo* synthesised component, characterised by deuterium incorporation levels ranging from 1 to 5 (M1-M5) and displayed in lighter shades, and the pre-existing component that was not newly synthesised *i.e.,* without any incorporation of deuterium (M0), and is depicted in darker tones. In the table, molar percents of *de novo* synthesised TAG, measured as deuterium enrichment after D_2O incubation, were reported. *p <0.05; non-parametric test of the Mann Whitney ranks. FA, fatty acids; iCCA, intrahepatic cholangiocarcinoma; MON, monolayer; SPH, sphere cultures; TAG, triglycerides; MFI, Mean Fluorescence Intensity.

acquired from m/z 60–1,050. Data analysis and isotopic natural abundance correction were performed using MassHunter Profinder (version 10.0.2). Data preprocessing was performed using the Batch Targeted Feature Extraction algorithm and

Agile 2 algorithm. This software assigned identities to metabolites by searching against an in-house compound database built with Agilent PCDL Manager (version B.08.00) based on the metabolite formula and its corresponding retention time with a score >75. Peak areas obtained were normalised for protein content for each sample. LC-MS analysis was performed by the Metabolomics Unit of JRU ISBE-SYSBIO Center and Elixir European Infrastructure in Milan (Milan, Italy).

In vivo experiments

Animal experiments were performed in accordance with national guidelines and approved by the ethical committee of the Animal Welfare Office of Italian Health Ministry. All procedures conformed to the legal mandates and the Italian guidelines for the care and maintenance of laboratory animals. All animals received humane care, and the study protocols complied with the institutional guidelines. Studies involving animal experiments conformed to the Animal Research: Reporting of In Vivo Experiments (ARRIVE) guidelines (http://www.nc3rs.org.uk/arriveguidelines), developed by the National Centre for the Replacement, Refinement and Reduction of Animals in Research (NC3Rs) to improve the standards and reporting of animal research. Male 6-week-old NOD/SCID mice (n = 6 per group) (Charles River Laboratories International, Wilmington, Massachusetts, MA, US) were subcutaneous injected with 3 × 10^6 CCLP1 SPH cells. When tumours became palpable, mice were randomly divided into two experimental groups to receive intraperitoneal injection of solution (10% DMSO, 40% PEG300, 5% TWEEN80, and 45% saline) or 240 mg/kg orlistat (three times a week). Animals were monitored daily. In parallel, we performed subcutaneous xenografts using injected CCLP1 cells (3 × 10^6) silenced for

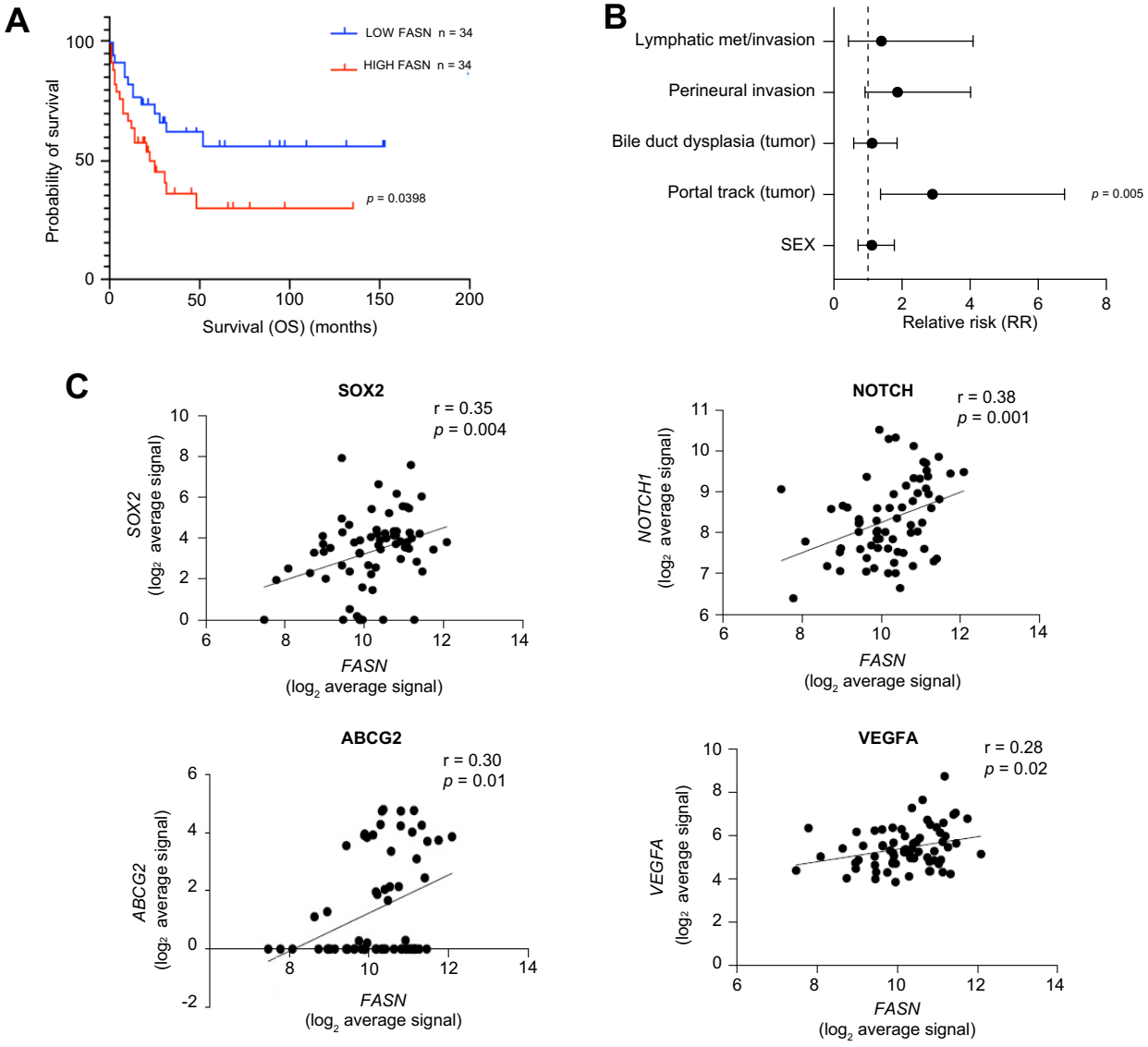

Fig. 6. Expression of Fatty acid synthase is associated with poor survival in iCCA patients. (A) Kaplan–Meyer plot showing overall survival in iCCA patients (n = 68) stratified according to good or bad prognosis. (B) Univariate association of FASN expression with clinical pathological parameters. (C) Scatterplot representing the correlation between *FASN* and *SOX2*, *NOTCH*, *ABCG2* and *VEGF* expression in a public dataset.[17] FASN, Fatty acid synthase; iCCA, intrahepatic cholangiocarcinoma; OS, overall survival.

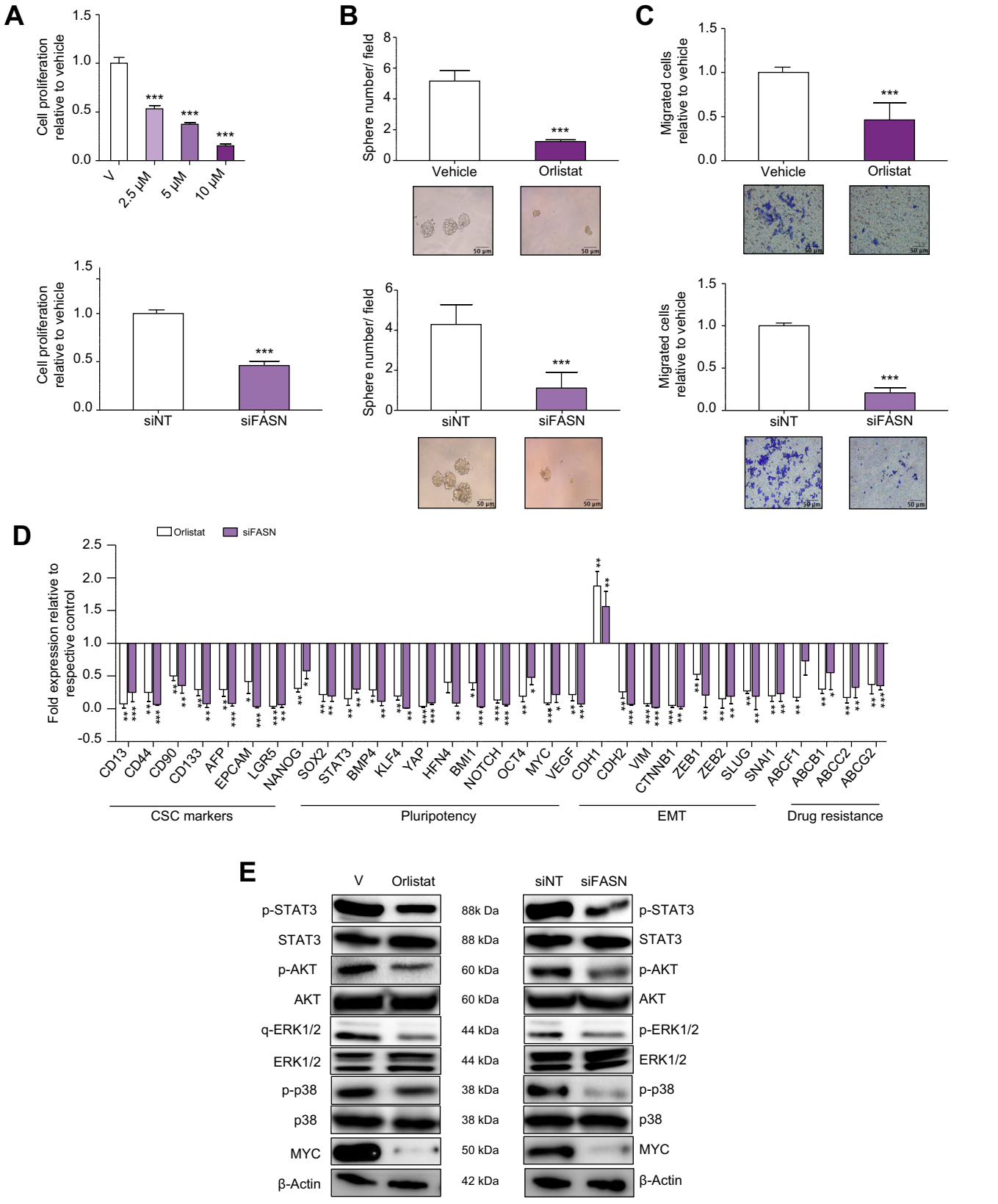

Fig. 7. Effects of FASN depletion in CCLP1 SPH. (A) Effect of FASN depletion on proliferation by BrdU incorporation 48 h after orlistat treatment (upper panel) or gene silencing (lower panel). Mean ± SEM (n = 3, ***p ≤0.001). (B) Effects of orlistat (upper panel) or FASN gene silencing (lower panel) on iCCA sphere forming efficiency. Mean ± SEM (n = 3, ***p ≤0.001; Mann–Whitney U test). Representative images of iCCA SPH are shown below the graphs (original magnification 40×). (C) Migration of orlistat treated SPH (upper panel) or FASN silenced SPH (lower panel) was measured in modified Boyden chambers. The number of migrated cells is represented as fold increase with respect to vehicle. Mean ± SEM (n = 3, ***p ≤0.001; Mann–Whitney U test). Representative images of filters are shown below the

FASN (SPH-T shFASN) expression or cells transfected with shCTR (SPH-T shCTR) (male 6-week-old NOD/SCID mice (n = 6 per group) (Charles River Laboratories International, Wilmington, Massachusetts, MA, US).

Statistical analysis

Statistical tests were performed using GraphPad Prism v.9 software, Boston, Massachusetts, MA, US and R version 4.1.0. software Indianapolis, Indiana, IN, US. For each experiment, statistical details can be found in the figure legends, including the statistical tests applied and the sample sizes. All *in vitro* experiments were confirmed by independent biological replicates. Data is represented as mean ± SD or ± SEM. Group comparison was performed using the nonparametric Mann–Whitney *U* test. Clinical data were examined using Fisher's exact test. The Kaplan–Meier method was employed to determine survival rates, with significance assessed using the Log-rank test. Pearson's correlation was utilised to assess the relationship between gene expression.

Detailed information is provided in the Supporting Information and in the Supplementary CTAT Table.

Results

Fatty acids enhance the stemness features of iCCA cells

To assess the relevance of FA in the biology of iCCA stem cells, CCLP1 and HUCCT1 cells were first exposed to increasing concentrations of unsaturated (oleic acid [OA], palmitoleic acid (POA], linoleic acid) or saturated (palmitic acid) FA for different time periods (Figs. S1 and S2, Tables S1 and S2). In line with previous studies,[14] all tested FA promoted cell growth (Figs. S1 and S2, Tables S1 and S2). Thus, based on the highest proliferative effect (Figs. S1 and S3), we focused our study on the role of OA and POA in the modulation of iCCA stemness.

Since CSC are key players in tumorigenesis including tumour initiation and metastasis, we next evaluated whether FA are able to modulate these aspects *in vitro* by reprogramming parental cells grown in MON cultures. Indeed, treatment of MON cells (HUCCT1 or CCLP1) with OA or POA markedly enhanced their sphere-forming ability (i.e. sphere number, volume, and growth over time) as an indication of self-renewal potential (Fig. 1A, Fig. S4A and B), significantly increased aldehyde dehydrogenase activity, serving as a functional marker of tumour stemness (Fig. S4C) and the notably improved the capacity to invade a basement-like membrane (Fig. 1B, Fig. S5). Accordingly, the expression of multiple genes implicated in the maintenance of stemness, self-renewal, and regulation of epithelial-to-mesenchymal transition (EMT) were modulated in a pro-malignant fashion (Fig. 1C), thus further supporting the *in vitro* functional importance of FA in acquiring a stem-like traits. Conversely, due to their drug-resistance, cancer stem cells can escape cytotoxicity and survive chemotherapy and radiotherapy. Therefore, we assessed the influence of monounsaturated FA on iCCA resistance to chemotherapeutic agents. Pre-treatment with OA or POA before exposure to cisplatin, oxaliplatin, or gemcitabine, commonly used drugs for iCCA therapy,[1] led to a significant rescue of cell viability under pharmacological treatment as shown by analysis of apoptosis (Fig. 2, Fig. S6, Table S3).

The fatty acid metabolic machinery was enhanced in CCA stem-like cells

Based on the observed enrichment of stem cell properties *in vitro* in MON cells treated with exogenous OA or POA, we further investigated the metabolic apparatus of FA in the SPH culture system. This system functions as a model of tumour stemness in CCA, as previously described by our group[1] and confirmed at the molecular level by RNA-sequencing profiling of SPH cells (Fig. S7, Table S4). Utilising Enrichr analysis, we observed a significant enrichment of stem-related molecules among the differentially expressed genes in SPH compared to MON in both cell lines. The acquisition of stemness was further supported by the predominant activation of stem cell signalling pathways, including PI3K/Akt-, Hippo-, and TGF-beta-dependent pathways. Additionally, there was an upregulation of significant networks associated with the EMT process, TNF-alpha signalling via NF-kB, the p53 pathway, as well as factors related to pluripotency, stemness, and EMT, such as *POU5F1, STAT3, EZH2, ZEB1, MYC, SOX2,* and *ZEB2* genes (Fig. S7, Table S4).

Gene set enrichment analysis (GSEA) of SPH RNA sequencing data indicated a marked increase in the expression of several genes participating in FA metabolism, including both anabolic and catabolic pathways (Fig. 3A). Accordingly, an unsupervised clustering heatmap indicated a primary divergence in the expression pattern of differentially expressed genes involved in FA metabolism comparing SPH with MON culture systems for both cell lines (Fig. 3B). Furthermore, overexpression of key enzymes involved in FA synthesis (FASN, SREB, ACSL1, SCD1), desaturation (SCD1), and exogenous uptake (CD36, FATP4) was further confirmed at the mRNA level in SPH cells compared to MON cells (Fig. 3C). Of note, protein members of the mTOR signalling pathway and key metabolic enzymes involved in *de novo* fatty acid biosynthesis (cytoplasmic acetyl-CoA synthetase [AceCS1], ATP citrate lyase [ACLY], Acetyl-CoA carboxylase [ACAC] the rate-limiting step in FA synthesis, FASN, Acyl-CoA synthetase long chain family member 1 (ACSL1) were upregulated in SPH with respect to MON cultures of both CCLP1 and HUCCT1 cells lines, as shown by Western blotting analysis and the relative densitometric analysis (Fig. 3D, Fig. S8). Notably, it is well known that mTOR stimulates *de novo* lipogenesis via a SREB-dependent pathway through S6K phosphorylation.[16]

Based on this evidence, the content of selected intracellular free FAs in iCCA stem-like cells was quantified by LC-MS. Notably, an abundance of citric acid, a precursor of FA as well as POA, stearic acid, and OA was identified in SPH cells compared to the respective MON in both cell lines (Fig. 4) in accordance with molecular data (Fig. 3) showing differences in the expression of key enzymes of FA biosynthesis. Coherently,

barograms (original magnification 40×). (D) Expression of different genes involved in CSCs pathways, EMT and drug resistance expressed as fold changes normalised to mean expression of the respective vehicle. Mean ± SEM (n = 3, *$p \leq 0.05$, ** $p \leq 0.01$, *** $p \leq 0.001$; Mann–Whitney *U* test). (E) Immunoblot of several proteins and phosphoproteins involved in cell proliferation and survival, following orlistat treatment or FASN silencing. β-Actin immunoblot was performed to ensure equal loading. EMT, epithelial to mesenchymal transition; FASN, Fatty acid synthase; iCCA, intrahepatic cholangiocarcinoma; V, vehicle; CSC, cancer stem cells.

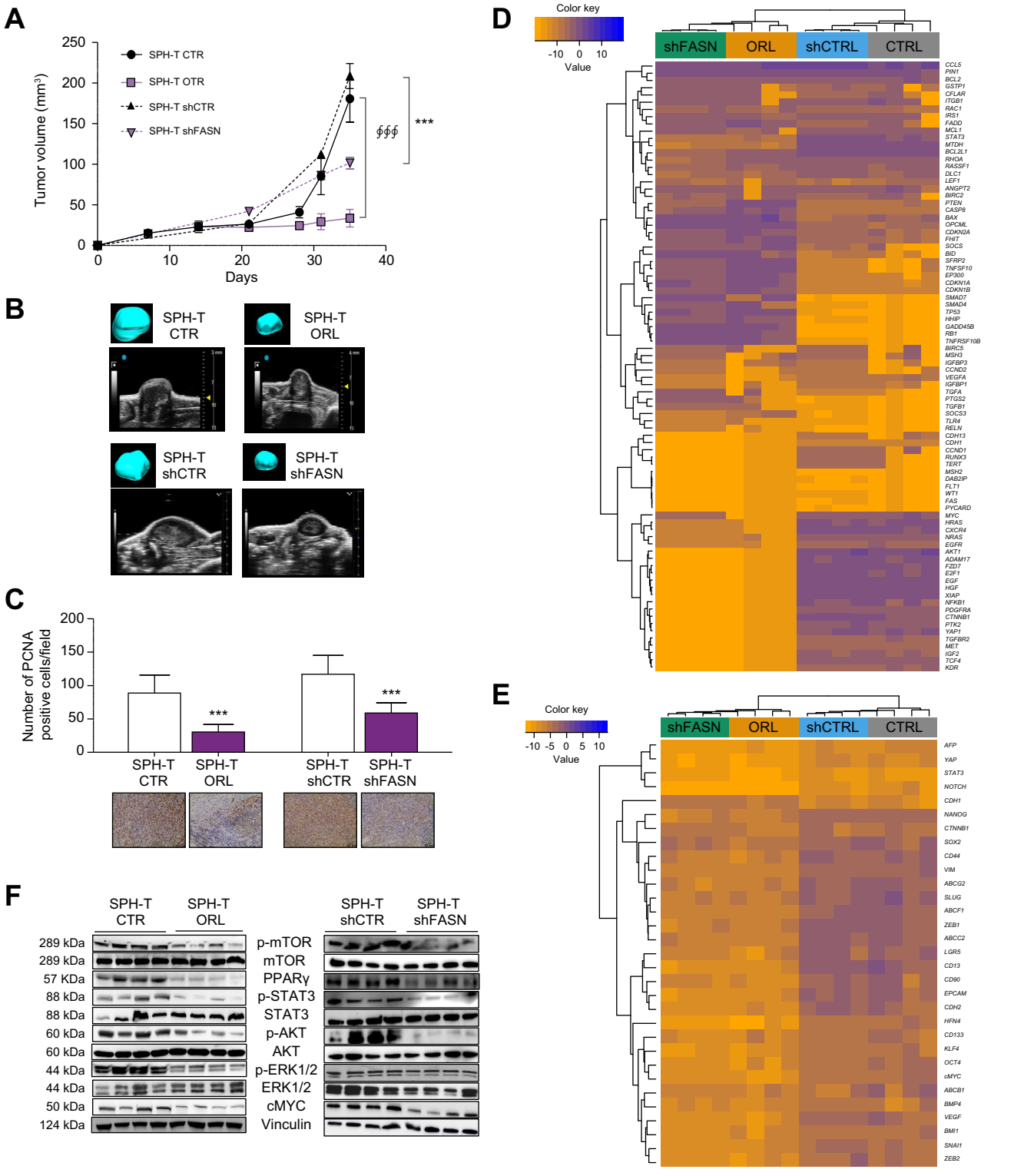

Fig. 8. Effects of orlistat treatment in iCCA xenografts mouse model. (A) Analysis of tumour volume by Vevo LAZR-X photoacoustic imaging. Tumours (SPH-T) were obtained by subcutaneous injection of SPH cells in NOD/SCID mice. Mice were treated with vehicle (SPH-T CTR) or orlistat (240 mg/kg/day) (SPH-T ORL) (n = 6 per group) or injected with FASN silenced SPH cells (SPH-T shFASN) or cells transfected with shCTR (SPH-T shCTR) ($^{\phi\phi\phi}p \leq 0.001$ SPH-T ORL *vs*. SPH-T CTR; SPH-T shFASN *vs*. SPH-T shCTR $^{***}p \leq 0.001$; Mann–Whitney *U* test). (B) Ultrasound images of representative subcutaneous tumour masses derived from injection of CCLP1 SPH generated tumours in different conditions. Three-dimensional rendering of the tumour mass is shown in the inset. (C) PCNA and haematoxylin eosin co-staining by immunohistochemical analysis. Representative staining is shown below the histogram. Ki67 positive nuclei are in brown colour ($^{***}p \leq 0.001$; Mann–Whitney *U* test). (D and E) Heatmap of different tumour samples based on qRT-PCR of arrays of genes focused on liver cancer pathways (84 genes) or cancer stem-like markers (31 genes). Gene expression levels are expressed as $\log_2$ transformed values in colour code from blue (low) to orange (high) according to the colour key scale bar.

BODIPY staining showed that iCCA-SPH had a higher amount of lipid droplets, which are dynamic organelles constituted mainly by triglycerides containing FA with different degrees of saturation or size (i.e. number of carbons due to elongation) (Fig. 5A and B).

Therefore, an untargeted lipidomic analysis was performed using high-resolution MS and targeted quantification of the most relevant lipids. By comparing the amount and composition of triglycerides in SPH cultures and the respective parental cells grown as monolayers, we observed that iCCA-SPH were characterised by a higher TAG composition including saturated and monounsaturated fatty acids (i.e. TAG with 1–2 double bonds) with respect to MON (data not shown). This was particularly evident in HUCCT1 cells, although both SPH cultures contained TAG of lower length than MON cultures (i.e. TAG with less than 52 carbons). Incubation with deuterated water was used to quantify the contribution of FA from *de novo* lipogenesis (DNL) of single triglycerides species. Palmitic acid (C16:0) is the main product of DNL and can either be desaturated to POA (C16:1) or elongated to stearic acid (C18:0) that in turn can be desaturated to OA (C18:1). The iCCA-SPH culture exhibited a larger percentage of *de novo* synthesised triglycerides (Fig. 5C), as assessed through the measurement of incorporation of deuterium. Within TAGs with lower length, SPH contained more TAG with monounsaturated triglycerides than MON, i.e. TAGs with POA and OA FA (48:1, 50:1, 52:1, than TAG incorporating only saturated FA like palmitic and stearic acid, (48:0, 50:0, 52:0), as shown in Fig. 5C-D. Accordingly, the desaturation index, i.e. the ratio between triglycerides with one double bond in the FA chain and triglycerides without double bonds, indicated a larger amount of monounsaturated FA in SPH (Fig. S9).

We next evaluated the pathways responsible for FA metabolism. SPH cells were characterised by elevated activity of intracellular FA beta-oxidation (FAO) compared to MON cultures (Fig. S10). This observation was supported by the increased content in lipid droplets evident in CCA-SPH cultures (Fig. 5A and B). Collectively, these findings identify a distinct alteration in mitochondrial function within SPH compared to MON cultured cells, corroborated by a previous study from our group.[2] To provide a more comprehensive perspective, we explored the classification of patients with CCA based on stemness and FA metabolic pathways using publicly available datasets (GSE32879 and GSE89749). Gene expression profiles for GSE89749 and GSE32879 were obtained from the Gene Expression Omnibus. A curated list of stemness and chemoresistance genes, as well as Gene Ontology FAO and KEGG Biosynthesis of unsaturated fatty acids (DNL) terms were used in the analysis. Within each dataset, samples underwent z-scoring and hierarchical clustering based on the expression of stemness genes. Next, GSEA was used to establish the association of clusters with chemoresistance, DNL, and FAO. Hierarchical clustering allowed a clear definition of two clusters (A and B), based on the expression of 139 resistance and stemness genes (resistance&stemness signature). In each dataset, Cluster B was significantly enriched in the expression of stemness and resistance genes that was validated with GSEA (Figs. S11 and S12). In both GSE32879 and GSE89749 datasets, Cluster B was enriched in both FAO and DNL, suggesting positive association of stemness and FAO and stemness and DNL. Taken together, these data suggest that the stem-like subset has an amplified machinery for FA metabolism in iCCA.

Higher expression of FASN was associated with a more aggressive course in patients with iCCA

To explore the possible relevance of our *in vitro* data with the clinical setting, we analysed transcriptomic data from a published cohort of patients with iCCA to search for possible correlations between genes implicated in FA metabolism and clinical outcomes.[17] In particular, we focused our attention on the *FASN* gene, the master regulator of FA synthesis, which was upregulated in SPH compared to MON iCCA cultured cells. Clustering data based on *FASN* expression, Kaplan–Meyer curves demonstrated that higher FASN was strongly associated with significantly lower survival (Fig. 6A), in accordance with recently published data.[13] Notably FASN levels correlated with available clinical pathological parameters (Table S5) in particular with portal trunk invasion, a significant adverse prognostic factor in iCCA (Fig. 6B). In addition, FASN expression significantly correlated with a number of stemness-related genes including *SOX2, NOTCH1* and *ABCG2* in the same iCCA dataset (n = 68) (Fig. 6C).

FASN promotes the growth of experimental iCCA and confers stem cell features to the tumour

Based on the results of transcriptomic analysis in patients, we next investigated the effect of genetic (siRNA) or pharmacological inhibition of FASN in SPH cells. Drug inhibition was performed using orlistat, an anti-obesity drug that irreversibly inhibits the enzymatic activity of FASN.[18–22] Both specific genetic depletion (siRNA) (Fig. S13) or enzymatic inhibition (orlistat) of FASN in SPH cells significantly reduced *in vitro* functionally properties such as proliferation, sphere-forming ability, invasion, as well drug-resistance.[13] (Fig. 7A–C; Figs. S13 and 14). At the molecular level, FASN reduction impaired the expression of several key genes implicated in pluripotency (i.e. *NANOG, SOX2, KLF4, OCT4, BMI1*), drug resistance (ABC transporters) and EMT (*CHD2, VIM, ZEB1, ZEB2, SNAI1*), and impact the phosphorylation of pro-survival proteins (i.e. AKT, p38 and ERK1/2), as well as expression of MYC oncoprotein (Fig. 7D and E) (Tables S6, S7).

Based on the strong *in vitro* data indicating the involvement of FASN in the features of iCCA stem compartment relevant for tumour progression, we evaluated the possible impact of the inhibition of this protein in an *in vivo* model of CCA. To this aim, the effect of both orlistat pharmacological treatment and genetic FASN inhibition (shRNA) was investigated in a mouse xenograft model in which dissociated CCLP1 SPH cells were injected subcutaneously into the flank(s) of NOD/SCID mice.[2]

Hierarchical clustering was based on complete linkage on Euclidean distances between genes (rows) or samples (columns). (F) Immunoblot of several proteins involved in proliferation and survival in tumour samples. Vinculin immunoblot was performed to ensure equal loading. FASN, Fatty acid synthase; iCCA, intrahepatic cholangiocarcinoma; SPH-T, tumors obtained by subcutaneous injection of SPH cells; CTR, control; ORL, orlistat; SPH-T shFASN, tumor derived by FASN silenced SPH cells; SPH-T shCTR, tumor derived by control silenced SPH cells.

After confirming that treatment with orlistat at a dose of 240 mg/kg/day was not toxic (Fig. S15A) and in accordance with previously reported studies,[18,21,22] mice were randomised once the tumour was palpable and treated with orlistat via i.p. injection (SPH-T ORL) or vehicle (SPH-T CTR) for 4 weeks. In parallel, we performed subcutaneous xenografts using CCLP1 cells silenced for FASN (SPH-T shFASN), or cells transfected with shCTR (SPH-T shCTR) after confirming FASN depletion at the protein level (Fig. S15B). Tumour growth was monitored with a dedicated *in vivo* imaging system. Tumour volume and weight in the ORL-treated and shFASN groups were significantly reduced compared with SPH-T CTR and SPH-T shCTR, respectively (Fig. 8A and B, Fig. S15C), while no differences in liver/body weight or in lung/body weight ratios were observed (Fig. S15D and E). At the end of treatment, *in vivo* cell proliferation was evaluated by PCNA staining (Fig. 8C). Both SPH-T ORL and SPH-T shFASN showed a lower number of cycling cells, in agreement with the observed impact on tumour progression. Moreover, comparison of the molecular characteristics of the xenografts (Fig. 8D and E) revealed in both SPH-T ORL and SPH-T shFASN tissues a downregulation of genes involved in proliferation (i.e. *STAT3, MTDH, BCL2L1, XIAP, AKT, EGF, EGFR, E2F1, HGF, HRAS, IGF2, NRAS, PDGFRA, FZD7, PTK2, c-MYC*), invasion (i.e. *ZEB1, SLUG,* N-cadherin, beta-catenin*, ADAM17, CXCR4, FDZ7, MET, PTK2*), drug-resistance (*ABCG2, ABCF1, ABCC2*) and pluripotency (*NANOG, NOTCH, HNF4, KLF4*), cancer stem cell markers (*CD44, CD13, EpCAM*) together with upregulation of tumour-suppressor (i.e. *OPCML, TP53, HHIP, SMAD4, RB1, GADD45B, PTEN, SFRP2, SOCS3*) and proapoptotic genes (i.e. *FADD*, *CASP8, BAX,BUD, TNFRSF10B*) (Fig. 8E).

Accordingly, at the protein level, FASN inhibition and depletion were associated with a lower activation/expression of proteins involved in proliferation or survival (i.e. STAT3, AKT, ERK1/2, c-MYC) and anabolic pathways (mTOR and PPARγ) (Fig. 8F), confirming the key role of FASN and FA metabolism in tumour growth.

Discussion

Metabolic rewiring is a new hallmark of cancer, and in recent years has changed the view of tumour biology. Among several tumour metabolic alterations, lipid metabolism is receiving increasing attention, and several studies have demonstrated its central role in the process of carcinogenesis.[23] As major components of lipids, FA provide energy, membrane building blocks, signalling molecules and post-translational modifications of proteins that are determinants for cancer cell survival.

The present study provides several lines of evidence supporting the role of increased FA metabolism in conferring a stem-like phenotype in iCCA. Notably, exposure to mono-unsaturated FA increased stem-like features at both functional (resistance to antineoplastic drugs, spherogenicity) and molecular (expression of stemness-associated genes) levels. Taking advantage of a 3D SPH culture system as a model for cancer stem cells[1,2] and comparing these cultures with more differentiated parental cells grown in monolayers, we provide compelling evidence for the importance of FA in the regulation of the stemness features of iCCA. Several key enzymes involved in FA synthesis and transport were significantly overexpressed in the iCCA stem-compartment, indicating that a CSC phenotype is strictly associated with altered FA metabolism. Additionally, lipidomic analysis demonstrated that iCCA-SPH cultured cells exhibit higher *de novo* synthesis and desaturated FA that are then esterified to triglycerides, which then results in enrichment of monosaturated FA. This finding may suggest that *de novo* synthesis and desaturation of FA may have an essential role in fuelling the activation of pluripotency and self-renewal associated signalling networks contributing either reprogramming iCCA cells towards a less differentiated stem-like phenotype or favouring the expansion of the stem subpopulation by supporting their metabolism. In line with our results, a recently published study[14] highlighted the pathogenic role of FA, showing that an exogenous supply of FA modulated the growth of CCA cells. Unlike more differentiated tumour cells, enhanced FA biosynthetic apparatus of iCCA stem-like cells probably render them more independent from the external source.

Additionally, the increased expression of FASN, the key enzyme in FA synthesis, was correlated with shorter survival in a dataset of 68 patients with iCCA thus suggesting that tumours with a worse prognosis are characterised by an increased content of intracellular FA. This might be potentially interesting considering our *in vitro* evidence of increased drug-resistance after exposure to FA. However, a detailed analysis of the underlying FA-driven molecular mechanism(s) is needed to provide the underlying mechanisms involved in the effective acquisition of a pharmacologically-resistant iCCA phenotype.

Nevertheless, we went further to demonstrate the functional relevance of FASN in stem-like iCCA cells both in the *in vitro* and *in vivo* settings. *In vitro*, FASN inhibition with both orlistat and specific gene silencing induced a significant decrease in pluripotency and stemness markers, as well as in the expression of genes involved in EMT and drug-resistance. These effects were replicated in a preclinical model of iCCA *in vivo*, where FASN inhibition caused a significant reduction in tumour growth after injection of resuspended iCCA-SPH. This was associated with dramatic changes in the expression of genes related to stemness and aggressiveness of iCCA. These data, together with those obtained in patients with iCCA, collectively indicate that tumour stem-like cells have distinct rearrangements of FA metabolism compared to more differentiated cells, and metabolic rewiring contributes to self-renewal and stemness maintenance with a major impact on the aggressiveness of iCCA cells.

Although the development and progression of cancer are frequently associated with increased *de novo* production of FA in several tumour types, the role of FASN in CCA is still controversial.[12–15] Indeed, several studies,[12] have shown that cholangiocarcinogenesis can be insensitive to FASN deprivation since CCA cells displayed enhanced FA uptake-related machinery. Differences observed in various studies may be ascribed to variances in patient cohorts, including different underlying aetiological factors (e.g. higher prevalence of MASLD, metabolic syndrome, or diabetes), and the intricate dynamics of the tumour microenvironment, especially the immune milieu. Furthermore, the diversity among liver tumour populations may result in variable reliance on FASN across cellular subsets. An additional explanation for these apparently divergent results can be that enhanced *de novo* lipogenesis and increased FASN expression are strictly related to the stemness component rather

than to the more differentiated iCCA cells. Moreover, the abnormally activated *de novo* synthesis of FA may contribute to satisfy the energy needs for the maintenance of a stemness state in iCCA, as also suggested by our previous study.[2] Thus, the results of the present study identify a new player in the regulation of lipid metabolism in iCCA with particular relevance to the biology of the stem cell compartment, and which could represent a target for treatment to be explored in dedicated studies. Of note, new FASN inhibitors are being developed, including TVB-2640, which is already being evaluated in clinical trials for the treatment of MASLD.[24]

An important aspect that will deserve additional research is related to the possible interaction between altered FA metabolism and metabolic disorders, such as MASLD, which are associated with an elevated risk of iCCA.[25–28]

Recently, it has been shown that metabolic disorders are associated with an elevated risk of intrahepatic CCA.[25–28] These metabolic risk factors encompass diabetes, obesity, metabolic syndrome and MASLD, which are frequently associated with dyslipidaemia. Unfortunately, the current datasets including clinical data do not specifically report the presence of MASLD, metabolic syndrome, or diabetes. However, it is imperative to investigate the potential presence and role of increased stemness in iCCA patients with these comorbidities. Further exploration and additional clinical data encompassing these specific aspects are warranted.

In conclusion, this study provides evidence that an altered FA metabolism contributes to the maintenance of stem-like phenotype in iCCA. These data allow to better understand the biology of CSCs in iCCA and suggest that inhibition of FASN may be a new potential target to interfere with tumour initiation of this deadly disease.

Affiliations

[1]*Department of Experimental and Clinical Medicine, University of Florence, Florence, Italy;* [2]*Department of Biomaterial Science and Technology, University of Twente Enschede, The Netherlands;* [3]*Department of Experimental and Clinical Biomedical Sciences, University of Florence, Florence, Italy;* [4]*Biotech Research and Innovation Centre, Department of Health and Medical Sciences, University of Copenhagen, Copenhagen, Denmark;* [5]*Department of Biotechnology and Biosciences, University of Milano-Bicocca, Milan, Italy;* [6]*Department of Pharmacy-Drug Sciences, University of Bari, Bari, Italy;* [7]*Department of Biosciences, Biotechnologies and Environment, University of Bari, Bari, Italy;* [8]*Cancer Genomics Lab, Fondazione Edo ed Elvo Tempia, Biella, Italy;* [9]*Institute of Clinical Physiology, National Research Council, CNR, Pisa, Italy*

Abbreviations

ACAC, Acetyl-CoA carboxylase; AceCS1, cytoplasmic acetyl-CoA synthetase; ACLY, ATP citrate lyase; ACSL1, Acyl-CoA Synthetase Long Chain Family Member 1; CCA, cholangiocarcinoma; CSC, cancer stem cells; DNL, *de novo* lipogenesis; EMT, epithelial to mesenchymal transition; FA, fatty acids; FAO, Fatty acids beta-oxidation; FASN, Fatty acid synthase; GSEA, gene set-enrichment analysis; iCCA, intrahepatic cholangiocarcinoma; LC-MS, Liquid chromatography-mass spectrometry; MASLD, metabolic dysfunction-associated steatotic liver disease; MON, monolayer; OA, Oleic Acid; POA, Palmitoleic Acid; SPH, sphere cultures; TAGs, triacylglycerols.

Financial support

Funding for this work was provided by grants from Associazione Italiana per la Ricerca sul Cancro (AIRC) (IG23117) to CR, (IG27094) to MLT, Cassa di Risparmio di Pistoia e Pescia, and the University of Florence to FM. JBA and CR are members of the European Network for the Study of Cholangiocarcinoma (ENSCCA) and participate in the initiative COST Action EURO-CHOLANGIO-NET granted by the COST Association (CA18122).

Conflicts of interest

The authors declare no competing interests.

Please refer to the accompanying ICMJE disclosure forms for further details.

Authors' contributions

Designed the study and wrote the manuscript: CR, FM. Provided materials, performed the experiments, collected the data, and analysed the results: GL, MP, NN, BP, RB, ER, IT, ML, JBA, TL, AA, MLT, EP, CM, CA, SM, ES, SR, AT, GA, MR, PO, CPN, MP, FC, SS, AG. Supervised the project and critically revised the manuscript: CR and MF. All authors read and approved the final manuscript.

Data availability statement

The data that support the findings of this study are available from the corresponding authors, upon reasonable request.

Acknowledgements

The authors thank Dr AJ Demetris (University of Pittsburgh, Pittsburgh, PA, USA) for cholangiocarcinoma cell lines (HUCCT1 and CCLP1).

Supplementary data

Supplementary data to this article can be found online at https://doi.org/10.1016/j.jhepr.2024.101182.

References

Author names in bold designated shared co-first authorship

[1] **Raggi C**, **Correnti M**, Sica A, et al. Cholangiocarcinoma stem-like subset shapes tumor-initiating niche by educating associated macrophages. J Hepatol 2017;66:102–115.

[2] Raggi C, Taddei ML, Sacco E, et al. Mitochondrial oxidative metabolism contributes to a cancer stem cell phenotype in cholangiocarcinoma. J Hepatol 2021;74:1373–1385.

[3] Raggi C, Factor VM, Seo D, et al. Epigenetic reprogramming modulates malignant properties of human liver cancer. Hepatology 2014;59:2251–2262.

[4] Banales JM, Marin JJG, Lamarca A, et al. Cholangiocarcinoma 2020: the next horizon in mechanisms and management. Nat Rev Gastroenterol Hepatol 2020;17:557–588.

[5] **Kuo CY**, **Ann DK**. When fats commit crimes: fatty acid metabolism, cancer stemness and therapeutic resistance. Cancer Commun (Lond) 2018;38:47.

[6] Mancini R, Noto A, Pisanu ME, et al. Metabolic features of cancer stem cells: the emerging role of lipid metabolism. Oncogene 2018;37:2367–2378.

[7] Yi M, Li J, Chen S, et al. Emerging role of lipid metabolism alterations in Cancer stem cells. J Exp Clin Cancer Res 2018;37:118.

[8] Begicevic RR, Arfuso F, Falasca M. Bioactive lipids in cancer stem cells. World J Stem Cells 2019;11:693–704.

[9] Noto A, De Vitis C, Pisanu ME, et al. Stearoyl-CoA-desaturase 1 regulates lung cancer stemness via stabilization and nuclear localization of YAP/TAZ. Oncogene 2017;36:4573–4584.

[10] **Li J**, **Condello S**, Thomes-Pepin J, et al. Lipid desaturation is a metabolic marker and therapeutic target of ovarian cancer stem cells. Cell Stem Cell 2017;20:303–314.e5.

[11] **Zhang H**, **Zhu K**, Zhang R, et al. Oleic acid-PPARγ-FABP4 loop fuels cholangiocarcinoma colonization in lymph node metastases microenvironment. Hepatology 2024;80:69–86.

[12] **Li L**, **Che L**, Tharp KM, et al. Differential requirement for de novo lipogenesis in cholangiocarcinoma and hepatocellular carcinoma of mice and humans. Hepatology 2016;63:1900–1913.

[13] Tomacha J, Dokduang H, Padthaisong S, et al. Targeting fatty acid synthase modulates metabolic pathways and inhibits cholangiocarcinoma cell progression. Front Pharmacol 2021;12:696961.

[14] Ruiz de Gauna M, Biancaniello F, González-Romero F, et al. Cholangiocarcinoma progression depends on the uptake and metabolization of extracellular lipids. Hepatology 2022;76:1617–1633.
[15] **Xu L**, **Zhang Y**, **Lin Z**, et al. FASN-mediated fatty acid biosynthesis remodels immune environment in Clonorchis sinensis infection-related intrahepatic cholangiocarcinoma. J Hepatol 2024;81:265–277.
[16] Peterson TR, Sen Gupta SS, Harris TE, et al. mTOR complex 1 regulates lipin 1 localization to control the SREBP pathway. Cell 2011;146:408–420.
[17] Andersen JB, Spee B, Blechacz BR, et al. Genomic and genetic characterization of cholangiocarcinoma identifies therapeutic targets for tyrosine kinase inhibitors. Gastroenterology 2012;142:1021–1031.e15.
[18] **Kridel SJ**, **Axelrod F**, Rozenkrantz N, et al. Orlistat is a novel inhibitor of fatty acid synthase with antitumor activity. Cancer Res 2004;64:2070–2075.
[19] **Peng H**, **Wang Q**, Qi X, et al. Orlistat induces apoptosis and protective autophagy in ovarian cancer cells: involvement of Akt-mTOR-mediated signaling pathway. Arch Gynecol Obstet 2018;298:597–605.
[20] **Zhang Q**, **Zhou Y**, **Feng X**, **Gao Y**, et al. Low-dose orlistat promotes the therapeutic effect of oxaliplatin in colorectal cancer. Biomed Pharmacother 2022;153:113426.
[21] **Zhang C**, **Sheng L**, **Yuan M**, et al. Orlistat delays hepatocarcinogenesis in mice with hepatic co-activation of AKT and c-Met. Toxicol Appl Pharmacol 2020;392:114918.
[22] **Seguin F**, **Carvalho MA**, Bastos DC, et al. The fatty acid synthase inhibitor orlistat reduces experimental metastases and angiogenesis in B16-F10 melanomas. Br J Cancer 2012;107:977–987.
[23] Baenke F, Peck B, Miess H, et al. Hooked on fat: the role of lipid synthesis in cancer metabolism and tumour development. Dis Model Mech 2013;6:1353–1363.
[24] Loomba R, Mohseni R, Lucas KJ, et al. TVB-2640 (FASN Inhibitor) for the treatment of nonalcoholic steatohepatitis: FASCINATE-1, a randomized, placebo-controlled phase 2a trial. Gastroenterology 2021;161:1475–1486.
[25] **Da Fonseca LG**, **Hashizume PH**, de Oliveira IS, et al. Association between metabolic disorders and cholangiocarcinoma: impact of a postulated risk factor with rising incidence. Cancers (Basel) 2022;14.
[26] **Park JH**, **Hong JY**, Park YS, et al. Persistent status of metabolic syndrome and risk of cholangiocarcinoma: a Korean nationwide population-based cohort study. Eur J Cancer 2021;155:97–105.
[27] **Yugawa K**, **Itoh S**, Iseda N, et al. Obesity is a risk factor for intrahepatic cholangiocarcinoma progression associated with alterations of metabolic activity and immune status. Sci Rep 2021;11:5845.
[28] **Cadamuro M**, **Sarcognato S**, Camerotto R, et al. Intrahepatic cholangiocarcinoma developing in patients with metabolic syndrome is characterized by osteopontin overexpression in the tumor stroma. Int J Mol Sci 2023;24.

Keywords: Hepatobiliary tumours; Cancer stem cells; Lipid metabolism; Oleic acid; Palmitoleic acid; triglycerides; Lipid droplets.
Received 5 August 2023; received in revised form 26 July 2024; accepted 30 July 2024; Available online 6 August 2024

Journal of Hepatology, Volume *6*

Supplemental information

Altered fatty acid metabolism rewires cholangiocarcinoma stemness features

Giulia Lori, Mirella Pastore, Nadia Navari, Benedetta Piombanti, Richell Booijink, Elisabetta Rovida, Ignazia Tusa, Monika Lewinska, Jesper B. Andersen, Tiziano Lottini, Annarosa Arcangeli, Maria Letizia Taddei, Erica Pranzini, Caterina Mancini, Cecilia Anceschi, Stefania Madiai, Elena Sacco, Stefano Rota, Adriana Trapani, Gennaro Agrimi, Matteo Ramazzotti, Paola Ostano, Caterina Peraldo Neia, Matteo Parri, Fabrizia Carli, Silvia Sabatini, Amalia Gastaldelli, Fabio Marra, and Chiara Raggi

Altered fatty acid metabolism rewires cholangiocarcinoma stemness features

Giulia Lori, Mirella Pastore, Nadia Navari, Benedetta Piombanti, Richell Booijink, Elisabetta Rovida, Ignazia Tusa, Monika Lewinska, Jesper B. Andersen, Tiziano Lottini, Annarosa Arcangeli, Maria Letizia Taddei, Erica Pranzini, Caterina Mancini, Cecilia Anceschi, Stefania Madiai, Elena Sacco, Stefano Rota, Adriana Trapani, Gennaro Agrimi, Matteo Ramazzotti, Paola Ostano, Caterina Peraldo Neia, Matteo Parri, Fabrizia Carli, Silvia Sabatini, Amalia Gastaldelli, Fabio Marra, Chiara Raggi

Table of contents

Supplementary materials and methods

Cell culture and reagents

CCLP1, HUCCT1 and SG231 cells, from intrahepatic bile duct cancer tissue, were kind gift from Dr. AJ Demetris, University of Pittsburgh. iCCA4 were provided by Prof Domenico Alvaro Sapienza University of Rome, Italy. Cell lines were cultured as described (1,2). BSA, oleic acid, palmitoleic acid, fluorescein 5(6)-isothiocyanate (FITC) were purchased from Sigma Aldrich. Orlistat was purchased from MedChem Express. Dialysis tubes with a MWCO 1200-14000 Da were purchased from Spectra Labs (Rome, Italy).

Sphere formation assay

The cells were grown in anchoring-independent conditions into poly 2-hydroxyethyl methacrylate (poly-HEMA)-coated dishes (Sigma Aldrich) with selective serum-free DMEM/F12 medium supplemented with 1X B27 supplement without vitamin A (Life Technologies), 20 ng/mL EGF, and 20 ng/mL bFGF (R&D Systems) (1, 2). To determine SPH-forming ability, 500 CCA cells/well in a 96 multiwell were grown in anchoring-independent conditions with selective serum-free medium. After 7 days, pictures were taken to measure the number and size of CCA-SPH using a Leica DMi1microscope (Leica). Average number of formed spheres microscopic field (20x) over five fields. CCA-SPH volume was calculated after measuring length 1 (L1) and the length 2 (L2) using the following formula: V = (L1*L2*L2)/2.

Quantitative real-time polymerase chain reaction (RT-PCR)

Total RNA was extracted with the RNeasy kit (Qiagen) according to the manufacturer's instructions. The RNA concentration and quality were determine using an optical NanoDrop ND1000 spectrophotometer (ThermoFisher Scientific). Total RNA (1 µg) was retro transcribed with a High-Capacity cDNA Reverse Transcription Kit (Applied Biosystems). Relative gene expression was calculated using $2^{-\Delta\Delta Ct}$ method. The mRNA levels of Actin were used for normalization. Results shown are the mean of three different experiments ± SD. Sequences of used primers are listed in Supplemental Table 6.

Western blot analysis

Cells were lysed at 4°C with lysis buffer (1% Triton X-100, 50 mmol/L Tris–HCl, pH 7.4, 150 mmol/L NaCl, 1 mmol/L EDTA, 1 mmol/L sodium orthovanadate, 2 mmol/L PMSF, and 1 mmol/L each of leupeptin and pepstatin). After 30 minutes of lysis, cellular extracts were centrifuged for 20 min at 14000 rpm, and the supernatant was used for Western blot experiments as detailed elsewhere (2). Antibodies were used according to the manufacturer's

instructions. Immunoblot were incubated overnight at 4°C with primary antibody in 1% BSA in PBS. Primary antibodies are listed in Supplemental Table7.

Then, immunoblot were incubated with secondary antibody α-rabbit/mouse (1:4000) in 1% BSA in 1x DPBS for 1hour, then with Horseradish peroxidase (HRP)-conjugated tertiary antibody α-rabbit/mouse Monoclonal anti-β-actin antibodies produced in mouse (A5441, Sigma) or monoclonal anti-vinculin antibodies produced in mouse (V9131, Sigma) were used as internal control (1:1000). Quantification of the signal was obtained by chemiluminescence detection on an Image Quant Las4000 (GE Healthcare Life Sciences) and subsequent analysis conducted with ImageJ software.

Cell survival assay

A total of $8x10^4$ CCA cells were seeded in 96 multiwell plate and serum starved for 24h. Then cells were treated with oleic or palmitoleic acid for 24 hours and with cisplatin or oxaliplatin for further 24 hours. Medium was removed and a 0.5% crystal violet solution in 20% methanol was added. After 5 min of staining, the fixed cells were washed with phosphate-buffered saline (PBS) and solubilized with 100 µl/well of 0.1 M sodium citrate, pH 4.2. The absorbance at 595 nm was evaluated using a microplate reader (HiPo biosan, Bio Class).

Annexin V/PI staining

A total of $1x10^5$ CCA cells were seeded in 6 multiwell dishes and serum starved for 24h. Then cells were treated with oleic or palmitoleic acid for 24h and with cisplatin or oxalilplatin for further 24hours. Cells were detached, counted and stained with Annexin V-FLUOS Staining Kit according to the manufacturer's instructions. The percentage of both early and late apoptotic cells were detected and measured using FACSCanto II (BD Biosciences).

Cell cycle analysis

In total, 80 000 cells/well were seeded in 6 multiwell dishes and exposed to the appropriate conditions. After medium removal, 400 µl of solution containing 50 µg/mL propidium iodide, 0.1% w/v trisodium citrate and 0.1% NP40 was added. Samples were then incubated for 30 min at 4°C in the dark and nuclei analyzed with an FACSCanto II (BD Biosciences).

Cell proliferation assay

A total of $10x10^4$ cells were plated in 96 multiwell plate and incubated in medium deprived of serum for 24 hours. Cells were exposed to different stimuli and then proliferation was evaluated by BrdU incorporation using the Cell Proliferation ELISA-BrdU (colorimetric) Kit (Roche) according to the manufacturer's protocols. SPH were dissociated and seeded in a 96-well plate and allowed to grow overnight in SPH medium with 1% FBS.

Aldehyde Dehydrogenase (ALDH) activity detection

ALDH activity was measured in iCCA spheres with different treatments using Aldehyde Dehydrogenase Activity Colorimetric Assay kit (Merck) following manufacturer's instruction.

Migration assay

Migration was measured in Boyden chamber equipped with 8 μm pore filters (Millipore Corp) coated with rat tail collagen (20 μg/ml) (Collaborative Biomedical Products, Bedford, UK), as described in detail elsewhere (2). After six hours incubation at 37 °C, cells migrated to the underside of the filters were fixed, stained with Diff Quick, mounted and counted at 40X magnification. The values for migration were expressed as the average number of migrating cells per microscopic field over five fields. Each experiment was performed in triplicate.

Cell transfection

Control siRNA and siFASN were purchased from Dharmacon. Cells were transfected as previously described (2) using the Amaxa nucleofection technology (Amaxa) according to manufacturer's instructions. CCLP1 cells were transfected with FASN human shRNA plasmid (#TR313058, Origene) or scrambled shRNA (#TR30012, Origene) using Lipofectamine 3000 (Thermofisher) according to the protocol. Transfected cells were established by selection with Puromycin.

FAO assay kit

Fatty acid beta oxidation was measured with FAO assay kit (Assay Genie) following the manufacturer's protocols.

BODIPY staining

MON and SPH cells were stained with 2 μm BODIPY 493/503 (Cayman Chemicals) in the dark at 37°C for 15 mins. Cells were harvested by trypsinization, washed twice and analyzed by flow cytometry with FACSCanto II (BD Biosciences). For confocal microscopy, cells were incubated with 2 μm BODIPY and 5 μm Hoechst for 15 mins in the dark at 37°C. Then, cells were washed twice in PBS and fixed in 4% PFA for 15 minutes at room temperature. PFA was removed and viewed by a confocal microscope (TCS SP8; Leica).

Lipidomic analysis

For lipidomic analysis three replicates of each cell line (CCLP1 MON n=3, CCLP1 SPH n=3, HUCCT1 MON n=3, HUCCT1 SPH n=3) were cultured for 48 hours with a medium enriched with 10% deuterated water. About one million of cells were homogenized with 300 of methanol

µl (or the volume was adjusted according to the number of cells) and 20ul of the mix of internal standards were added to the sample. Samples were put on oscillating plate for 30 minutes at 4°C and centrifuged at 14000 rpm. After centrifugation, the methanol surnatant was transferred to the vials for injection and analysis. Lipid classes were separated with UHPLC 1290 Infinity (Agilent) equipped with ZORBAX Eclipse Plus C18 2.1x100mm 1.8 µm column (Agilent), and untarget acquisition of all lipids was performed by LC/MS-QTOF (Agilent UHPLC 1290 Infinity-6540 QTOF) in positive ion ionization. The concentrations of a selected panel of lipids previously found relevant for liver disease (3) were quantified with internal standard, i.e., TG (15:/15:0/15:0) (Larodan), Ceramide (d18:1/17:0), Sphingomyelin (d18:1/17:0), Lysophosphatidylcholine (17:0), Phosphatidylcholine (17:0/17:0), Phosphatidylethanolamine (17:0/17:0), Lysophosphatidylethanolamine (17:1) (Avanti Polar Lipids, Alabaster, AL). For heatmap representation, lipids concentration levels were scaled to zero mean and unit variance and reported as median within the four groups. *De novo* TAGs synthesis was evaluated by measurement the deuterium incorporation using isotopologue extraction in Agilent MassHunter Profinder B.08.00 software. *De novo* TAGs synthesis was reported as % of labeled TGs in the total amount of single species. Desaturation was evaluated as ratio between monounsaturated to saturated TAGs.

Gene expression

Total RNA (3 µg) from in vivo mouse tumors was reverse transcribed using QuantiNova Reverse Transcription kit (Qiagen). RT-PCR was performed using QuantiNova LNA PCR Focus Panel Human Liver Cancer 384-well plates (SBHS-133ZE, Qiagen). In each 384-well plate, a number of 4 different tumor samples for each group were tested for 84 genes specifically associated with liver cancer pathways. The expression values were calculated with the ΔΔCt method, using the average of ACTB, GAPDH, RPLP0 and HPRT1 as housekeeping genes as reference. A cutoff of at least 1.5-fold increases and 0.5-fold decreases were considered significant.

In addition, same tumor samples for each group were tested for 31 genes associated with stemness features (CSC, EMT and drug transporters; TableS2). Total RNA (1 µg) from in vivo mouse tumors was retro transcribed with a High-Capacity cDNA Reverse Transcription Kit (Applied Biosystems). Relative gene expression was calculated using $2^{-\Delta\Delta Ct}$ method. The mRNA levels of Actin were used for normalization. Data are mean ± SEM (n=3). A cutoff of at least 1.5-fold increases and 0.5-fold decreases were considered significant.

Immunochemistry staining

From the *in vivo* experiment, tumor samples for each group were tested for -PCNA expression. The histological analysis of tumor mass was performed as described below. Removed tumors

were fixed at 4°C in 10% neutral buffered formalin (BioOptica, Milan) for histological analysis performed on paraffin-embedded sections (5 μm). Immunohistochemistry was performed using the Leica BOND-MAX™ automated system (Leica Microsystems). The expression of mouse monoclonal anti-PCNA (#2586, 1:8000, Cell Signaling Technology) was evaluated. Slides were developed with 3′3-diaminobenzidine DAB (Leica Microsystems) and counterstained with hematoxylin. For antibodies used on mouse tissues, the blocking Mouse on Mouse (M.O.M.) basic kit (Leica Microsystem) was used according to the manufacturer's datasheet. All sections were examined using an optical microscope and photos were acquired using Leica Scanner Aperio CS2 (Leica).

Microarray Data Analysis

Correlation of FASN expression with survival was performed by stratifying 68 iCCA patients (4) by median expression of FASN and generation of Kaplan-Meier curves. Survival curves were compared with the log-rank test (Prism 9.4.1). Spearman correlation of FASN expression with SOX2, NOTCH1, VEGFA, and ABCG2 was performed using log2 transformed expression signals (Prism 9.4.1). The univariate association of FASN expression with clinical pathological was performed with Fisher's exact test for categorical parameters and t-test for continuous data in iCCA patients stratified by median FASN expression.

Ultrasound and photoacoustic in vivo imaging

Tumor volumes were determined in vivo imaging system (Vevo LAZR-X photoacoustic imaging). High-resolution ultrasound (US) imaging was done performing 3D acquisition in B-Mode on live mice, by using VevoLAZR-X imaging station (Fujifilm Visualsonics). The acquisitions to evaluate the tumor growth were performed weakly, starting from the day before the first treatment, until the experimental endpoint. During the analysis, mice were anesthetized with a continuous flow of isoflurane (initial induction at 4% and maintenance at 2%) and placed on a mouse handling table, heated at 37°C, in prone position. ECG, respiration rate and body temperature were monitored during the analysis. 55-MHz transducer was used for echography. Data obtained were analyzed using Vevo LAB software (Fujifilm Visualsonics) to measure the tumor volumes.

Library preparation and RNA-sequencing

Total RNA was isolated from cells using the miRNeasy Mini Kit (Qiagen) according to the manufacturer's protocol. Total-RNA-sequencing (RNA-seq) library preparation was performed starting from 100 ng of total-RNA with the SMARTer Stranded Total RNA Sample Prep Kit - Low Input Mammalian (Clontech-Takara). The libraries obtained were qualitatively and qualitatively assessed by using TapeStation 4200 (Agilent) and quantified by Qubit

Fluorimeter (ThermoFisher). Afterwards, they were multiplexed in an equimolar pool and sequenced on a NextSeq-500 Illumina Platform generating more than 60 million 75bp Paired End reads (bp-PE) per sample.

Reads preprocessing

Sequencing data was demultiplexed into separate, adapter free compressed fastq files using bcl2fastq v2.20.0.422 (Illumina, Inc.) and a reference sample sheet specifying for each sample the corresponding barcode. Reads were further processed using the fastp program (5) configured to use 20 threads for removing read pairs with at least 50% of bases with Q > 30, a minimal length of 70 bp, a complexity > 30%. No trimming was performed on reads.

Reads alignment, abundance estimation and differential analysis

Reads mapping was performed using the default options but specifying the --numGibbsSamples 500 and -validateMappings options, on a reference transcriptome composed by the union of the human cDNA and ncDNA available from Ensembl (assembly GRCh38.p13) indexed with a kmer size of 23 by Salmon v0.14.1 (6). Reads were imported into R using the tximport package (7) with the “Salmon” specific method. Gene level abundance was estimated from transcript level estimates using the summarizeToGene function of tximport working on a transcript to gene association table (further associating gene names for functional analysis, see below) obtained with Ensembl Biomart system (8) operating on Ensembl genes 98/GRCh38.p13 human genes. Data matrices were eventually converted in DEseq2 objects using the DESeqDataSetFromTximport function, specifying the SPH vs MON phenotypes as the design contrast.

Functional analysis

For the functional analysis of the experiment the GSEA 4.0.2 software by BROAD Institute was used (9,10) in the GSEAPreRanked mode using the Wald-statistic from the DESeq2 analysis as input metric for sorting. Gene lists were obtained from MSigDB 7.0 (11,12) and gene names were converted into Ensembl gene IDs using a simple perl script reading the same table produced by Biomart used for gene abundance estimation (see above). A selection of interesting gene sets from the different MSigDB collections (kegg, biocarta, gobp, hallmark, reactome) was obtained by a custom bash script that isolated those containing mitochondrial genes (GO:0005739:mitochondrion).

Enrichr enrichment analysis

Differentially expressed genes (DEGs) in sphere (SPH) compared to monolayer (MON) in common between the CCLP1 and HUCCT1 cells with a fold change > 2 (n=307) were used to

perform molecular function and pathway analysis by Enrichr enrichment analysis at https://maayanlab.cloud/Enrichr. The following libraries were used for the analysis: Kyoto Encyclopedia of Genes and Genomes (KEGG) pathway, MSigDB Hallmark 2020, the enrichment of transcription factors (TF) Perturbations. The p-values were calculated using Fisher exact test and corrected for multiple testing by Benjamini–Hochberg adjustment and pathways with an adjusted p-value < 0.05 were considered significant. The combined score of the pathway analysis (Table S4) is calculated using the Fisher exact test and the Z-score to sort the pathways.

Supplementary figures

Suppl.Fig.1

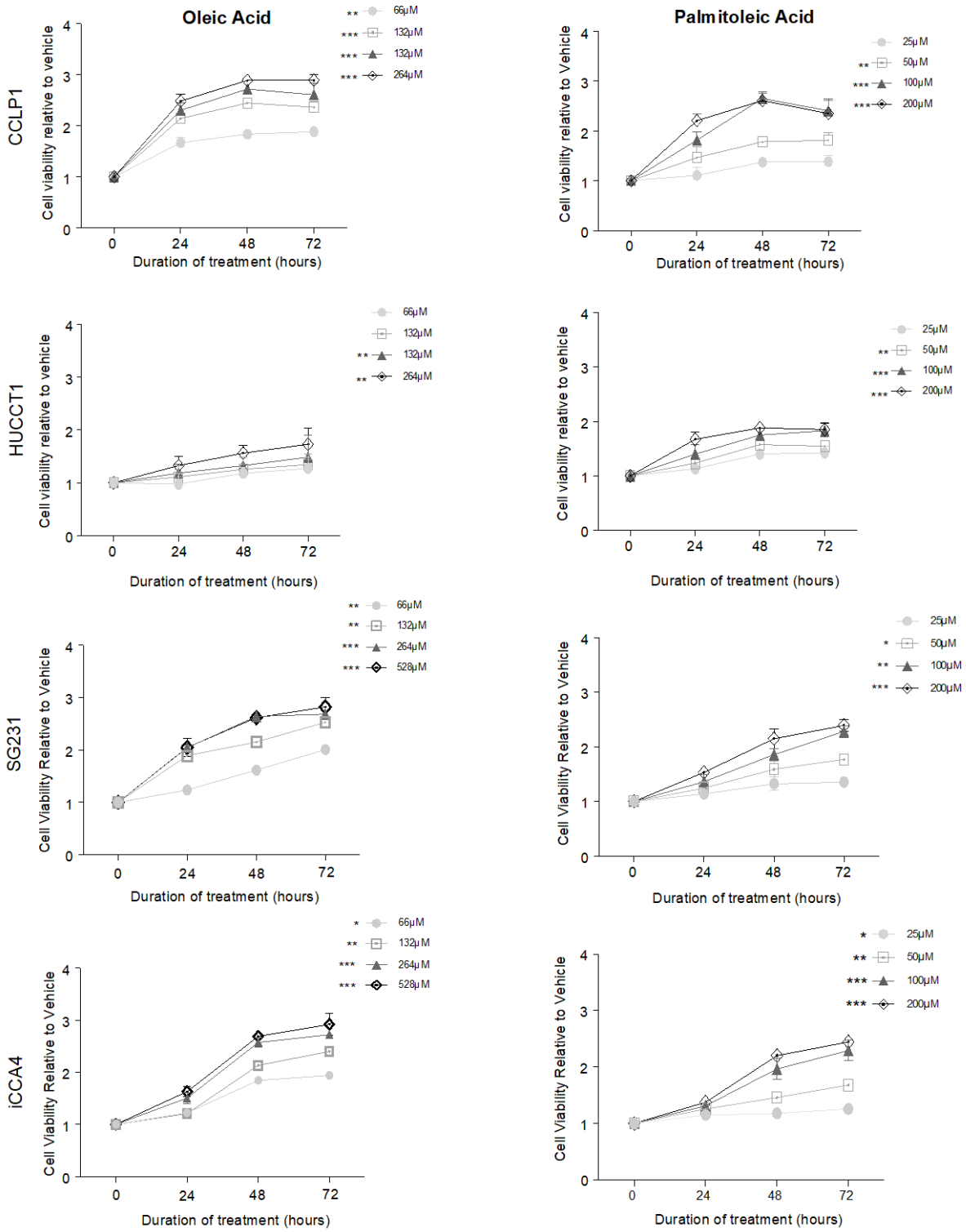

Fig. S1. Effects of oleic and palmitoleic acid on iCCA cells proliferation. Intrahepatic CCA cells were serum starved and treated with oleic or palmitoleic acid at the indicated concentration for 24, 48 and 72h in 4 iCCA cell lines (CCLP1, HUCCT1, SG231, iCCA). Then crystal violet test was performed. Results were normalized to vehicle: BSA for oleic acid and ethanol for linoleic, palmitic and palmitoleic respectively. Data are mean ± SEM (n=3, *p≤0,05, ** p≤0,01, *** p≤0,001; Mann-Whitney U test). Complete statistical data are shown in Supplementary Table 1.

Suppl.Fig.2

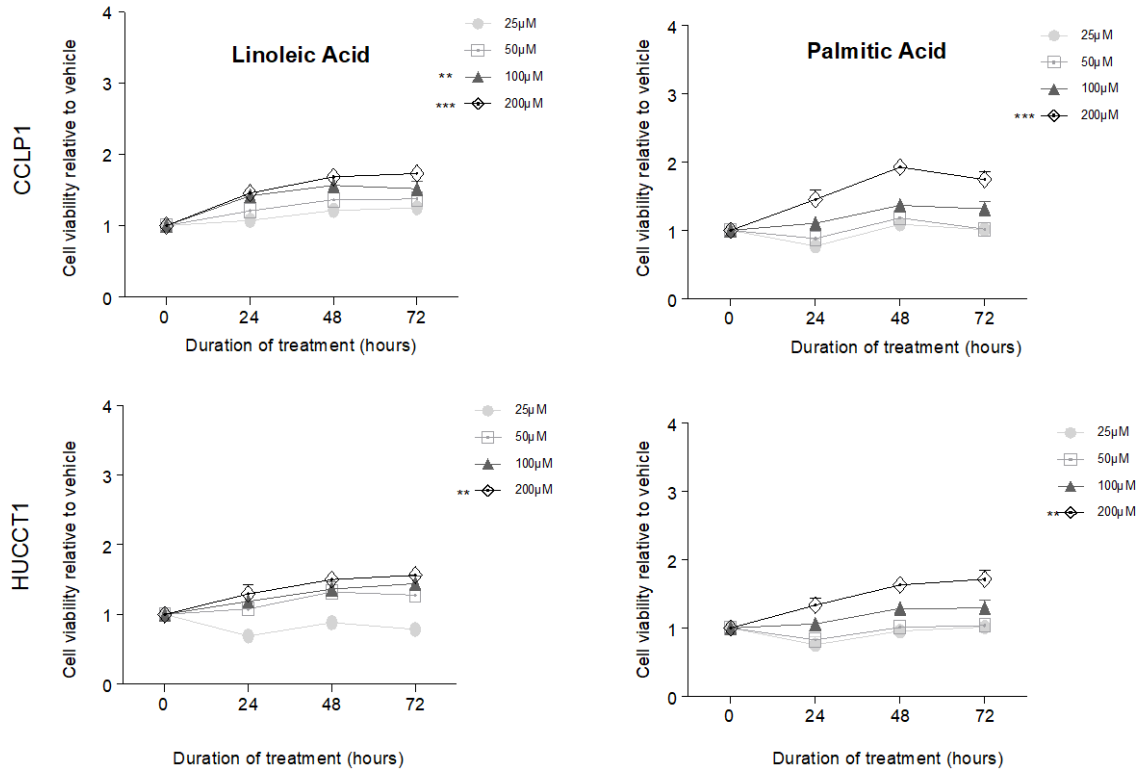

Fig. S2. Effects of linoleic and palmitic acid on iCCA cells proliferation. Intrahepatic CCA cells (CCLP1 and HUCCT1) were serum starved and treated with linoleic, palmitic, acid at the indicated concentration for 24, 48 and 72h. Then crystal violet test was performed. Results were normalized to vehicle: BSA for oleic acid and ethanol for linoleic, palmitic and palmitoleic respectively. Data are mean ± SEM (n=3, *p≤0,05, ** p≤0,01, *** p≤0,001; Mann-Whitney U test). Complete statistical data are shown in Supplementary Table 2.

Suppl.Fig.3

A

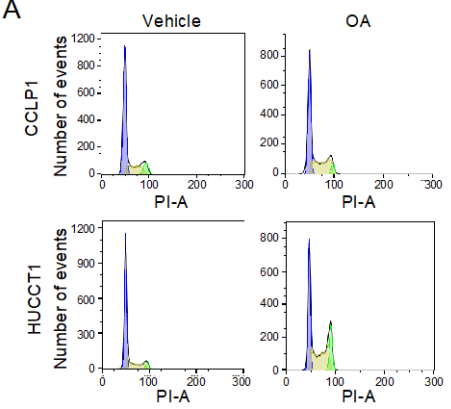

	CCLP1		HUCCT1	
	Vehicle	OA	Vehicle	OA
G0/G1	70.3 ± 9.6	59.0 ± 11.3	68.7 ± 1.1	44.6 ± 8.1**
S	19.9 ± 8.1	38.8 ± 13.0*	24.1 ± 1.3	40.2 ± 2.8***
G2/M	9.7 ± 7.9	2.2 ± 2.2*	7.2 ± 2.2	15.1 ± 5.3

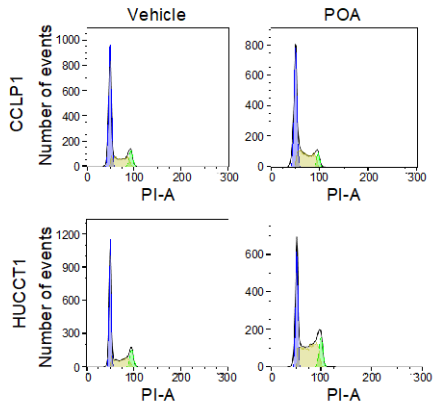

	CCLP1		HUCCT1	
	Vehicle	POA	Vehicle	POA
G0/G1	72.4 ± 11.6	49.0 ± 7.2**	53.3 ± 13.9	47.8 ± 9.7*
S	20.1 ± 12.4	42.0 ± 7.1**	28.7 ± 11.5	35.8 ± 11.9*
G2/M	7.5 ± 1.4	9.0 ± 3.3	14.2 ± 4.9	16.5 ± 6.7

B

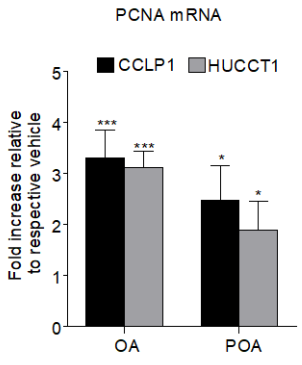

C

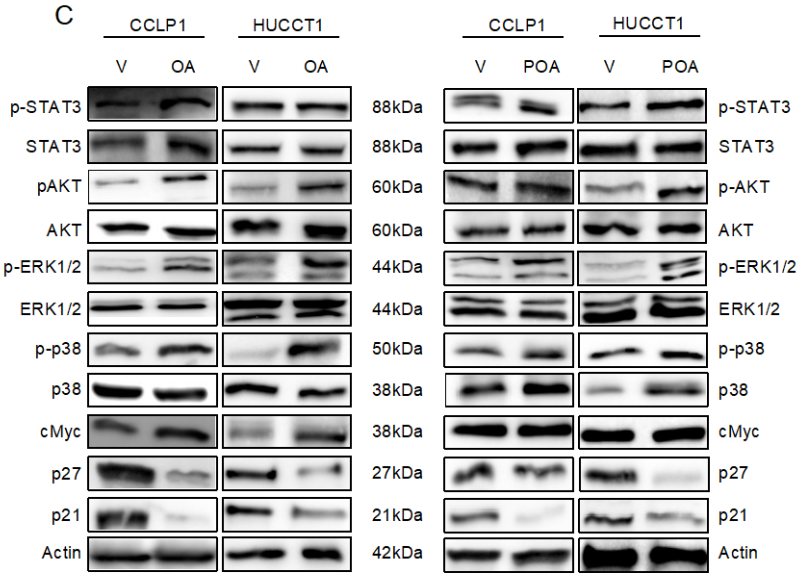

Fig. S3. Effects of monounsaturated fatty acids on cell cycle. (A) Intrahepatic CCA cells were treated in starvation medium for 48 hours with OA or POA. Cell cycle phase distribution was determined by flow cytometry. Data are mean ± SEM (n=4, *p≤0.05, **p≤0.01, *** p≤0,001; Mann-Whitney U test). (B) Intrahepatic CCA cells were treated with oleic or palmitoleic acid for 48h, then RNA was extracted. Expression of proliferating cell nuclear antigen (PCNA) gene is reported as fold changes normalized to mean expression of respective vehicle. Data are mean ± SEM (n=4, *p≤0,05, *** p≤0,001; Mann-Whitney U test). (C) Immunoblot of several proteins involved in proliferation and survival, after 48 hours MUFAs treatment in starvation medium. β-Actin immunoblot was performed to ensure equal loading.

Suppl.Fig.4

A

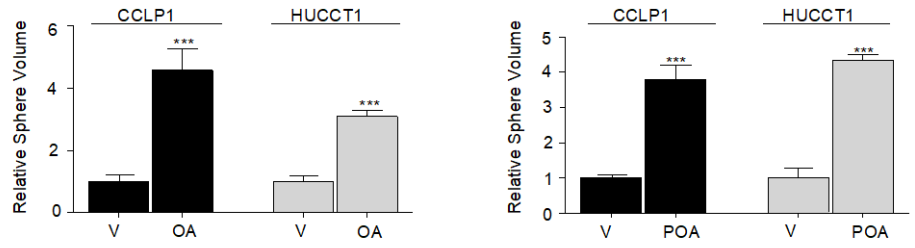

B

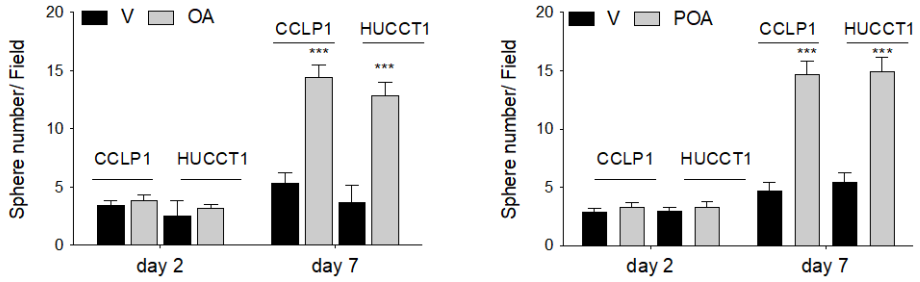

C

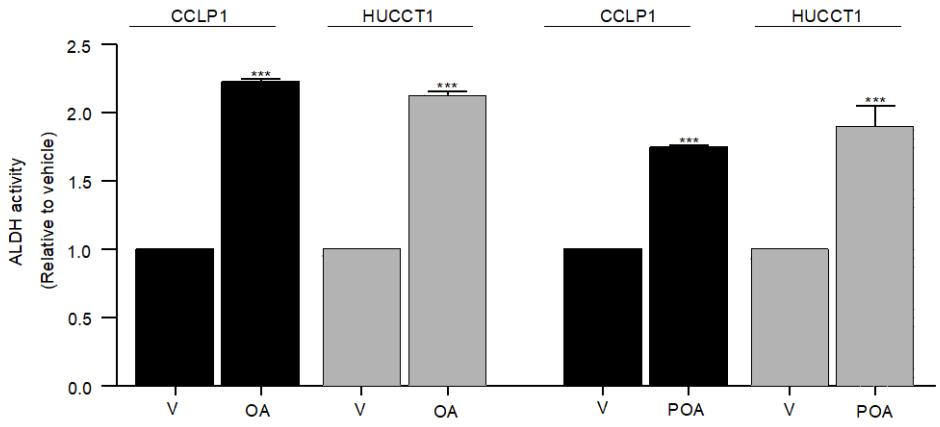

Fig. S4. Effect of MUFA on iCCA-stem-like properties. A) CCLP1 and HUCCT1 were grown as sphere (SPH) for seven days, then treated with OA or POA for 48 hours (during sphere formation). Cells have been synchronized in serum free condition, as required for cell cycle analysis. The impact of MUFAs treatment is reported as SPH volume relative to respective vehicle. Data are mean ± SEM (n=3, *** p≤0.001; Mann-Whitney U test). B) Intrahepatic CCA cells were grown were seeded in anchoring-independent conditions and treated with FAs for 48h. Then cells were grown as SPH for seven days. SPH were counted at days 2 (treatment starting) and at days 7 (end of experiment). Mean ± SEM (n=3, ***p≤0.001; Mann-Whitney U test). C) ALDH activity was determined in iCCA cells grown as SPH and treated with oleic or palmitoleic acid for 48h. Results were normalized to vehicle: BSA for oleic and ethanol for palmitoleic acid. Data are mean ± SEM (n=3, *** p≤0,001; Mann-Whitney U test).

Suppl.Fig.5

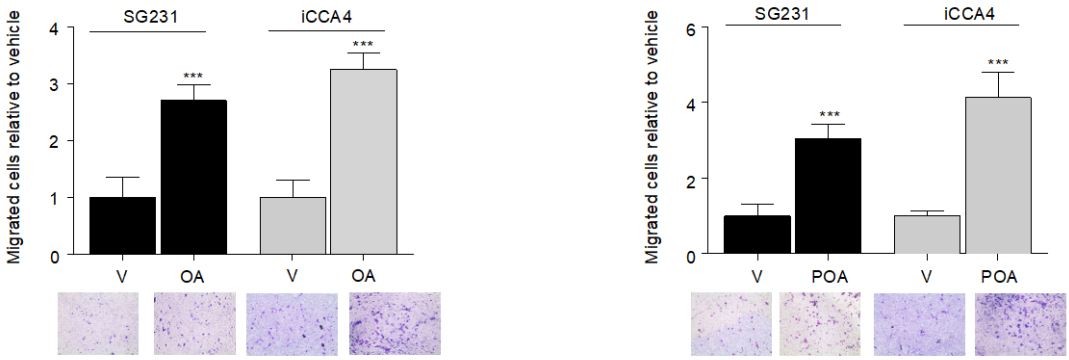

Fig. S5. Effects of oleic and palmitoleic acid on iCCA cell migration.

Migration of iCCA cells (SG231 and iCCA4) was measured in modified Boyden chambers, after 48 hours treatment. Mean ± SEM (n=3, ***p≤0.001); Mann-Whitney U test). Representative images of filters are shown below the barograms (original magnification 40x, scale bar 10µm).

Suppl.Fig.6

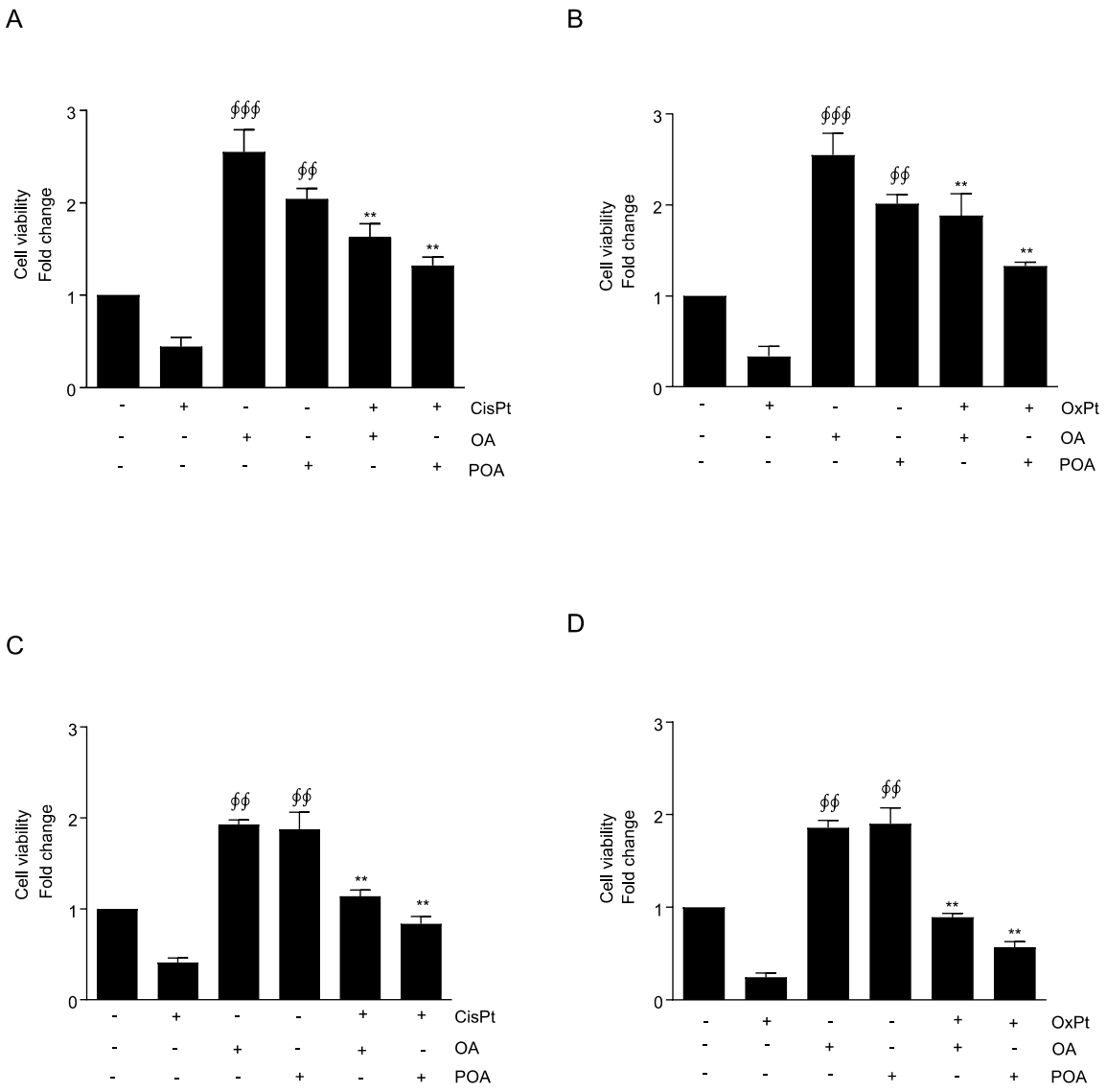

Fig. S6. **Monounsaturated FAs pretreatment protects iCCA cells from antiblastic toxic effects**. (A, B) CCLP1 and HUCCT1 cells were pretreated for 24 hours with oleic acid (OA) or palmitoleic acid (POA) in starvation medium, then with cisplatin or oxaliplatin for further 24 hours. Cell viability was assessed with crystal violet staining. Data are mean ± SEM (n=3, **p≤0.01, ***p≤0.001, ϕϕ p≤0.01, ϕϕϕ p≤0.001; Mann-Whitney U test). The * are calculated respect to cisplatin or oxalilplatin, ϕ are calculated respect to vehicle.

Suppl.Fig.7

A

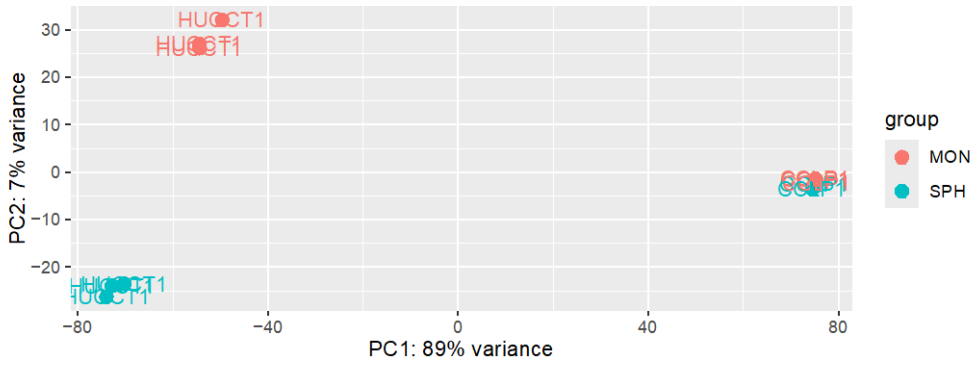

B

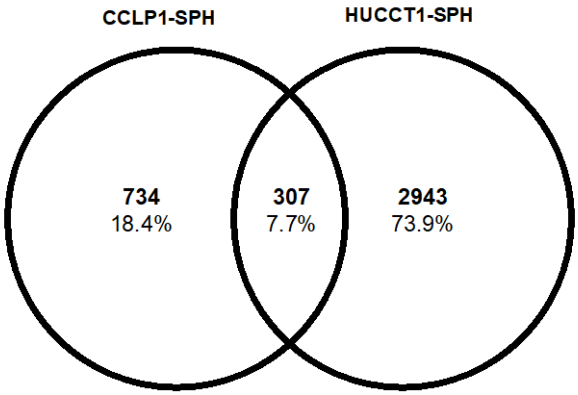

Fig. S7. Global molecular differences between sphere and monolayer cells by RNAseq analysis. A) Principal component analysis (PCA) of RNA sequeincig data of monlayer (MON) and sphere (SPH) in both CCLP1 and HUCTT1 cells. B) Venn diagram shows a total of 734 and 2943 differentially expressed genes (DEGs) in SPH compared to MON in CCLP1 and HUCCT1 respectively. Venn diagram software identified a total of 307 common DEGs in SPH.

Suppl.Fig.8

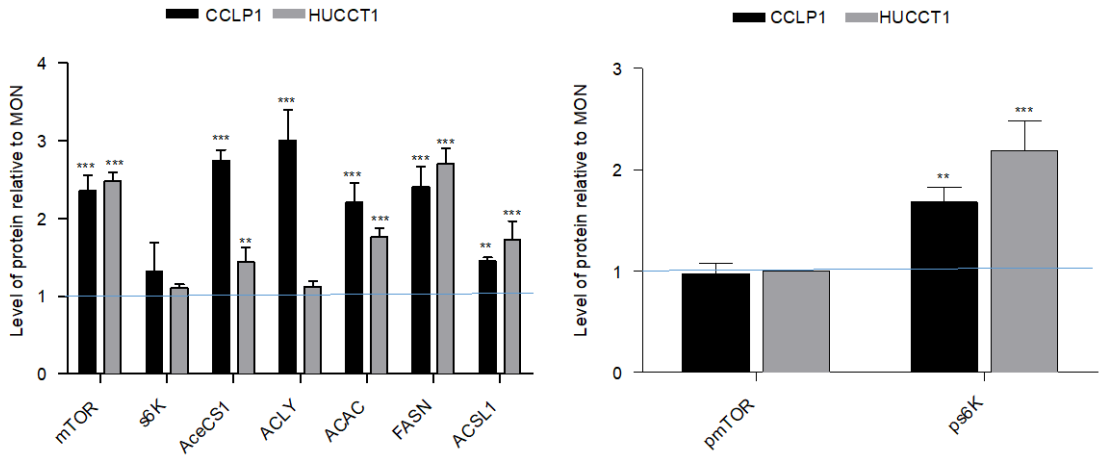

Fig. S8. Densitometric quantification of FA related proteins. Immunoblot quantification of mTOR, phospho mTOR, S6K, phosphoS6K, AceCS1, ACLY, ACAC, FASN, ACSL1 protein levels in CCLP1 and HUCCT1 cells grown as MON and SPH. mTOR, S6K, AceCS1, ACLY, ACAC, FASN and ACSL1 were normalized on β-Actin level, phospho mTOR and phosphoS6K were normalized on mTOR and S6K level, respectively. Data are shown as relative protein level respective to MON. Data are mean ± SEM (n=3, **p≤0.01, ***p≤0.001; Mann-Whitney U test).

Suppl.Fig.9

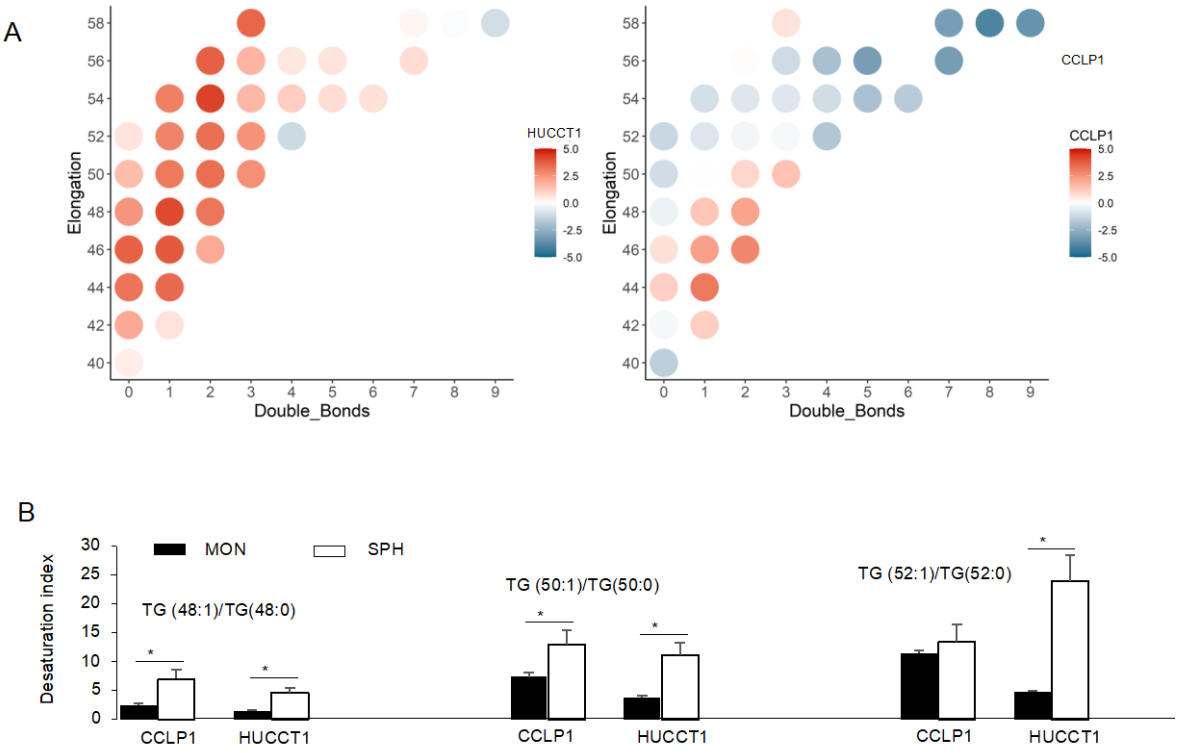

Fig. S9. Triglycerides elongation and desaturation in iCCA cells. (A) Fold change of elongation and number of double bonds of triglycerides in CCLP1 (SPH/MON) and HUCCT1 (SPH/MON). (B) Desaturation index in CCLP1 vs HUCCT1 calculated as the ratio between monounsaturated to saturated TG. Results are mean ± SEM (n=3, *p≤0,05; Mann-Whitney U test).

Suppl.Fig.10

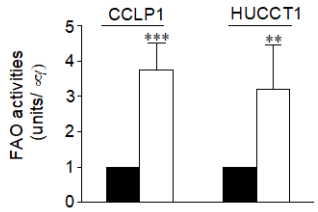

Fig. S10. Fatty acid oxidation in iCCA cells. CCLP1 and HUCCT1 cells were cultured as monolayer (MON) and sphere (SPH). Fatty acid oxidation activity was measured with a colorimetric kit. FAO was normalized on protein content measured by BCA assay. Data are mean ± SEM (n=3, **p≤0.01, *** p≤0.001; Mann-Whitney U test).

Suppl.Fig.11

A

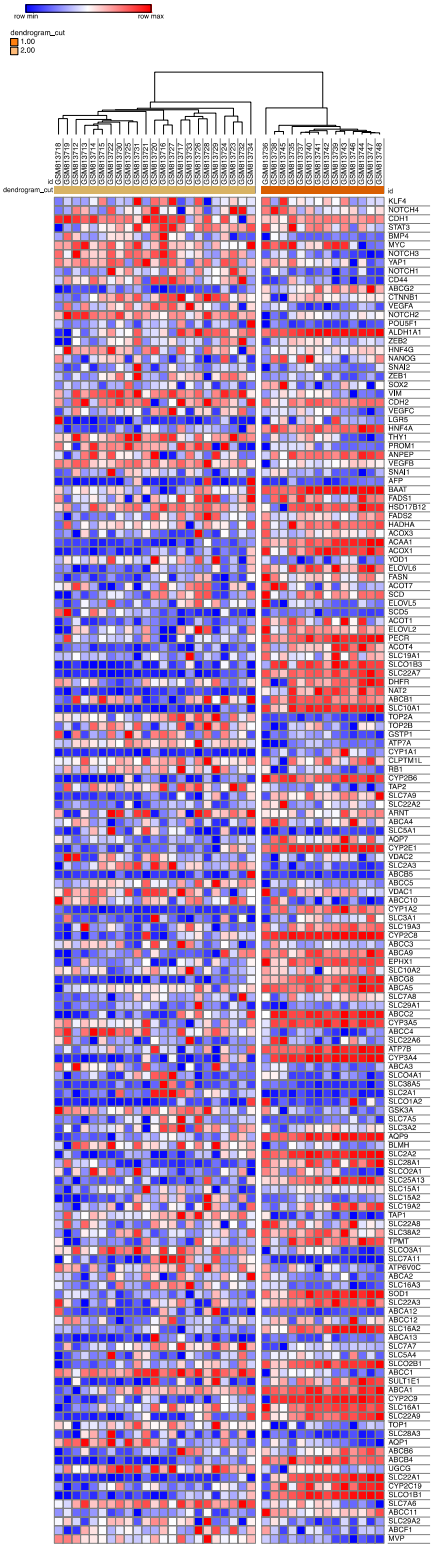

B

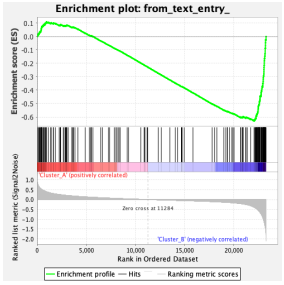

Normalized Enrichment Score (NES)=-1.67
Nominal p-value=0.002

C

FAO

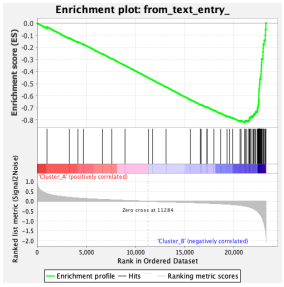

Normalized Enrichment Score (NES)=-1.64
Nominal p-value=0.002

DNL

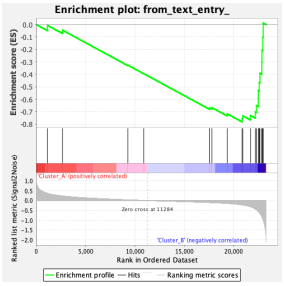

Normalized Enrichment Score (NES)=-1.48
Nominal p-value=0.021

Fig. S11. Classification of CCA patients in terms of stemness and the FA metabolic pathway activity by using public GSE32879 dataset. A) Based on the expression of 139 resistance and stemness genes, hierarchical clustering stratified patients into 2 clusters:
Cluster A: 20 samples, Cluster B: 17 samples. B) Cluster B shows significant enrichment of stemness and resistance genes that was validated with GSEA. C) Next, GSEA was used to associate clusters with curated *de novo* lipogenesis (DNL) and fatty acid beta-oxidation (FAO) gene sets. Both DNL and FAO signatures were significantly enriched in Cluster B. Normalized enrichment score (NES) and p value are reported

Suppl.Fig.12

A

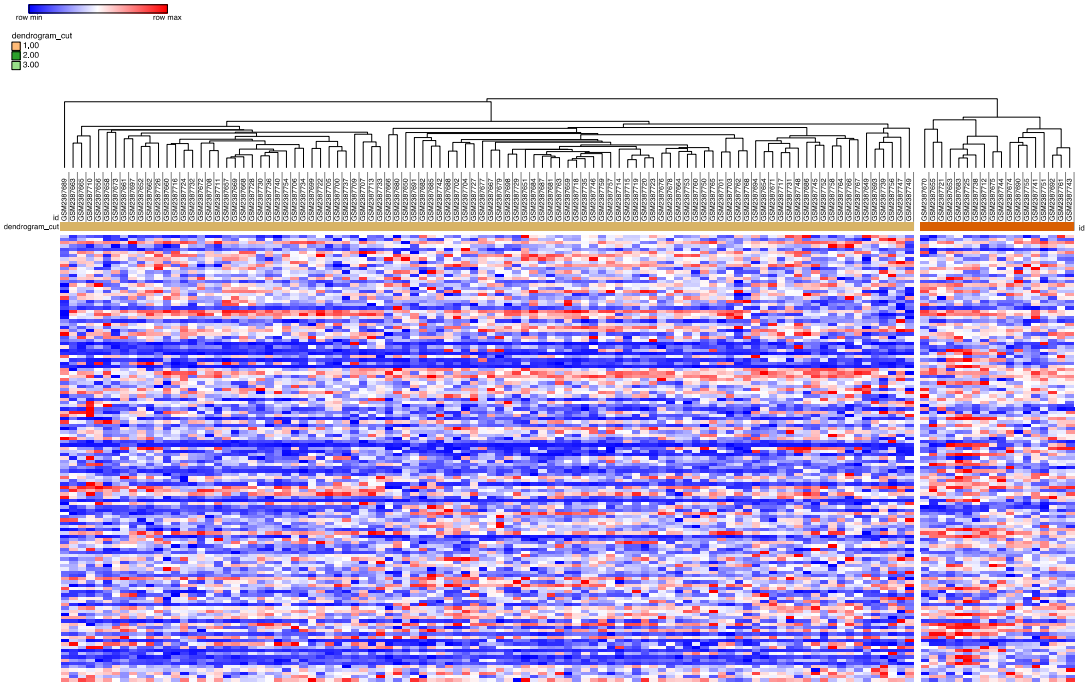

B

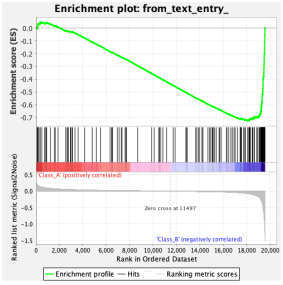

Normalized Enrichment Score (NES)=-1.82
Nominal p-value<0.0001

C

FAO

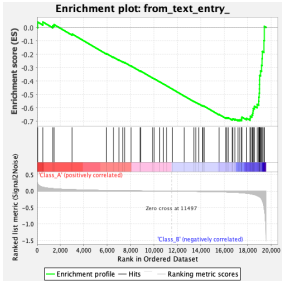

Normalized Enrichment Score (NES)=-1.78
Nominal p-value=0.002

DNL

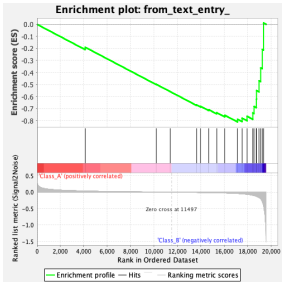

Normalized Enrichment Score (NES)=-1.72
Nominal p-value<0.0001

Fig. S12. Classification of CCA patients in terms of stemness and the FA metabolic pathway activity by using public GSE89749 dataset. A) Based on the expression of 139 resistance and stemness genes, hierarchical clustering stratified patients into 2 clusters: Cluster A: 100 samples, Cluster B: 18 samples. Cluster B shows significant enrichment of stemness and resistance genes that was validated with GSEA. C) Next, GSEA was used to associate clusters with curated *de novo* lipogenesis (DNL) and fatty acid beta-oxidation (FAO) gene sets. Both DNL and FAO signatures were significantly enriched in Cluster B. Normalized enrichment score (NES) and p value are reported

Suppl.Fig.13

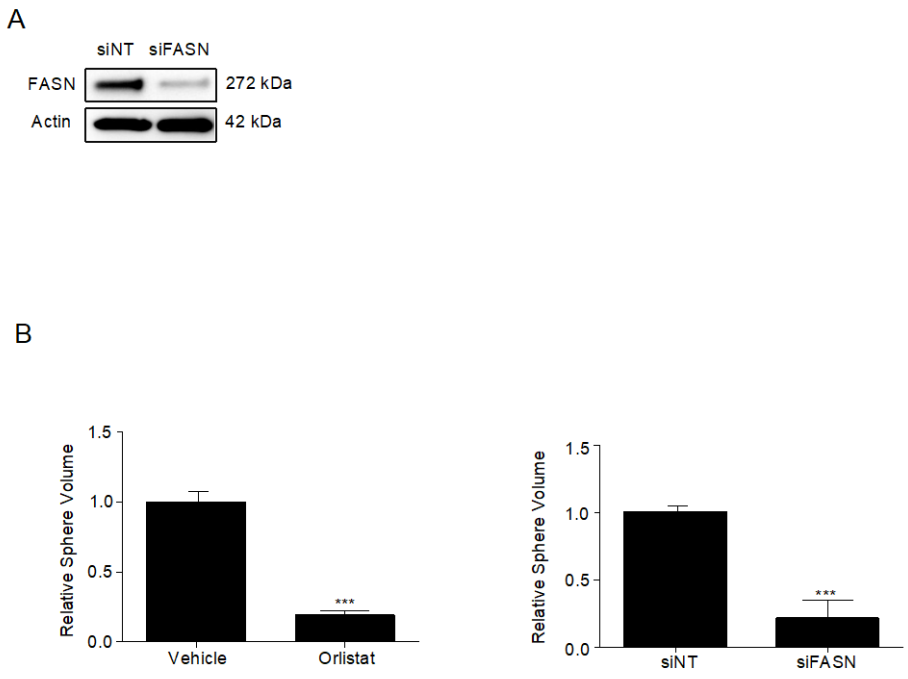

Fig. S13. FASN inhibition affects iCCA SPH forming efficiency. (A) Immunoblot of FASN in CCLP1 SPH transiently silenced for 48 hours. β-Actin immunoblot was performed to ensure equal loading. (B) CCLP1 cells were grown as spheroids for seven days, then treated with orlistat 10μM for 48h. The effect of FASN inhibition on SPH forming efficiency is reported as SPH volume. Data are mean ± SEM (n=3, *** p≤0.001; Mann-Whitney U test). (C) CCLP1 SPH were transiently silenced for 48hours, then cells were counted and sphere forming ability was measured.

Suppl.Fig.14

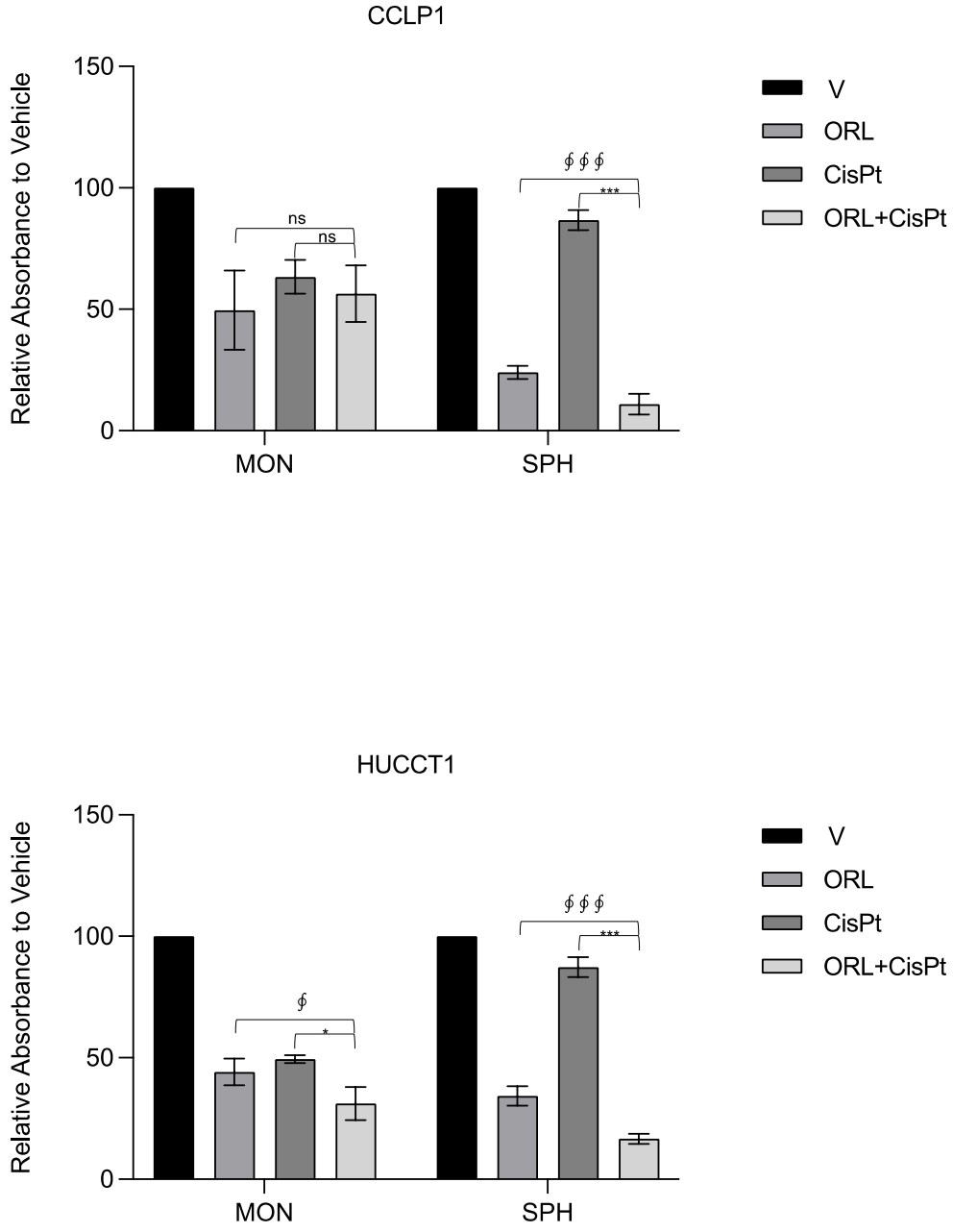

Fig. S14. Orlistat effect on chemoresistance of sphere and monolayer growth. Monolayer (MON) and dissociated sphere (SPH) cells were treated with orlistat (10μM) alone, cisplatin (6μM CCLP1; 15μM HUCCT1) alone and in combination. Cell viability was assessed with crystal violet staining. Data are mean ± SEM (n=3, *p≤0.5, ***p≤0.001, ϕ p≤0.5, ϕϕϕ p≤0.001; Mann-Whitney U test). The * are calculated respect to cisplatin (CisPt), ϕ are calculated respect to orlistat (ORL).

Suppl.Fig.15

A

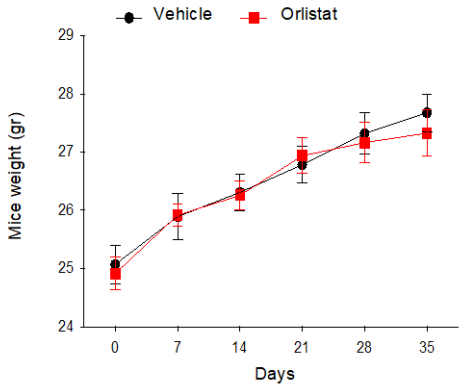

B

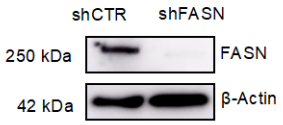

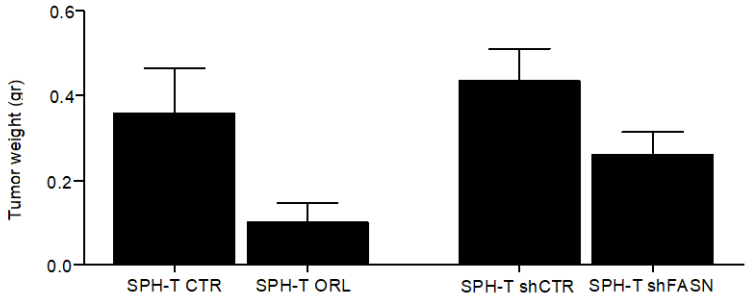

C

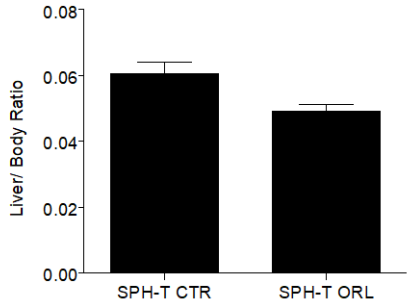

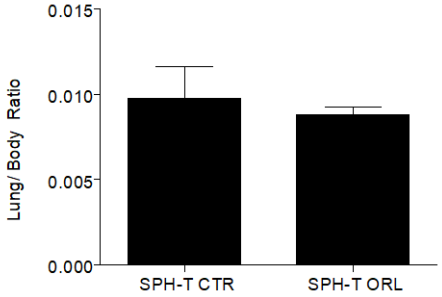

D

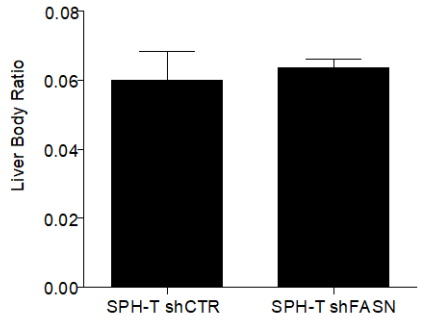

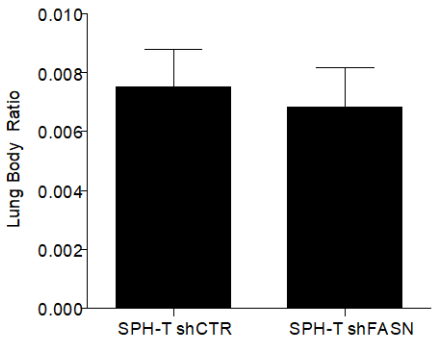

Fig. S15. *In vivo* effects of FASN inhibition. (A) body weight curve for both control and orlistat treated mice without tumor injection. (B) Immunoblot of FASN in CCLP1 SPH stable silenced with shRNA. β-Actin immunoblot was performed to ensure equal loading. Tumors, livers and lungs were collected and weighted at the end of the experiment. C) Weight of generated tumors at 5 weeks after subcutaneous injection into NOD-SCID mice of CCLP1 SPH (***p≤0.001; Mann-Whitney U test). (D,E) Evaluation of orlistat (SPH-T ORL, SPH-T CTR) and shFASN (SPH-T shFASN, SPH-T shCTR) side effects reported as liver body ratio and lung body ratio.

Supplementary tables

Table S1. Effects of fatty acids on iCCA cells proliferation

CCLP1

Oleic acid	24h	48h	72h
66µM	p<0,05	p<0,01	p<0,05
132µM	p<0,01	p<0,001	p<0,001
264µM	p<0,01	p<0,001	p<0,001
528µM	p<0,001	p<0,001	p<0,001

Palmitoleic acid	24h	48h	72h
25µM	ns	ns	ns
50µM	p<0,05	p<0,01	p<0,01
100µM	p<0,01	p<0,001	p<0,01
200µM	p<0,01	p<0,001	p<0,01

HUCCT1

Oleic acid	24h	48h	72h
66µM	ns	ns	ns
132µM	ns	ns	ns
264µM	ns	p<0,01	p<0,01
528µM	p<0,05	p<0,01	p<0,01

Palmitoleic acid	24h	48h	72h
25µM	ns	ns	ns
50µM	ns	p<0,01	p<0,05
100µM	ns	p<0,001	p<0,001
200µM	p<0,01	p<0,001	p<0,01

SG231

Oleic acid	24h	48h	72h
66µM	ns	p<0,05	p<0,05
132µM	p<0,01	p<0,01	p<0,001
264µM	p<0,001	p<0,001	p<0,001
528µM	p<0,001	p<0,001	p<0,001

Palmitoleic acid	24h	48h	72h
25µM	ns	ns	ns
50µM	ns	p<0,05	p<0,01
100µM	p<0,05	p<0,01	p<0,001
200µM	p<0,01	p<0,001	p<0,001

iCCA4

Oleic acid	24h	48h	72h
66µM	ns	p<0,05	p<0,05
132µM	ns	p<0,01	p<0,001
264µM	p<0,01	p<0,001	p<0,001
528µM	p<0,01	p<0,001	p<0,001

Palmitoleic acid	24h	48h	72h
25µM	ns	p<0,05	p<0,05
50µM	p<0,01	p<0,001	p<0,001
100µM	p<0,01	p<0,001	p<0,001
200µM	p<0,01	p<0,001	p<0,001

The table shows p values calculated on oleic or palmitoleic acid treatment for 24h, 48h and 72h in CCLP1, HUCCT1, SG231 and iCCA4 cells. Fatty acids concentrations are reported in the table. (*p≤0,05, ** p≤0,01, *** p≤0,001; Mann-Whitney U test)

Table S2. Effects of fatty acids on iCCA cells proliferation

CCLP1

Linoleic acid	24h	48h	72h
25uM	ns	ns	ns
50uM	ns	ns	ns
100uM	ns	p <0,01	p <0,01
200uM	p <0,05	p <0,001	p <0,001

Palmitic acid	24h	48h	72h
25uM	ns	ns	ns
50uM	ns	ns	ns
100uM	ns	p <0,01	p <0,05
200uM	p <0,01	p <0,001	p <0,001

HUCCT1

Linoleic acid	24h	48h	72h
25uM	ns	ns	ns
50uM	ns	ns	ns
100uM	ns	ns	p <0,01
200uM	ns	p <0,01	p <0,001

Palmitic acid	24h	48h	72h
25uM	ns	ns	ns
50uM	ns	ns	ns
100uM	ns	p <0,05	ns
200uM	p <0,05	p <0,01	p <0,01

The table shows p values calculated on linoleic or palmitic acid treatment for 24h, 48h and 72h in CCLP1, HUCCT cells. Fatty acids concentrations are reported in the table. (*p≤0,05, ** p≤0,01, *** p≤0,001; Mann-Whitney U test)

Table S3. Monounsaturated FAs pretreatment protects iCCA cells from antiblastic toxic effects

CCLP1

	Vehicle	CisPt	OA	POA	CisPt+OA	CisPt+POA
late	0,5%	36,9% ***	0%	1,5%	3,8% ϕϕ	1,8% ϕϕϕ
early	0,3%	8,9% ***	3%	1,5%	3,3% ϕ	3,2%

	Vehicle	OxPt	OA	POA	OxPt+OA	OxPt+POA
late	0,5%	43,7% ***	0%	1,5%	3,2% ϕϕ	1,7% ϕϕϕ
early	0,3%	7,6% ***	3%	1,5%	4,7%	1,3% ϕ

HUCCT1

	Vehicle	CisPt	OA	POA	CisPt+OA	CisPt+POA
late	3%	49,3% ***	3,2%	2,3%	9,4% ϕ	3,2% ϕϕ
early	3,7%	27,4% ***	7%	2,6%	17,2%	3,6% ϕϕ

	Vehicle	OxPt	OA	POA	OxPt+OA	OxPt+POA
late	3%	36% ***	3,2%	2,3%	8,8% ϕ	4,8% ϕϕ
early	3,7%	35% ***	7%	2,6%	9% ϕ	2,6% ϕ

The percentage of early or late apoptotic cells in CCLP1 and HUCCT1 cells treated as reported. **p≤0.01, ***p≤0.001, ϕϕ p≤0.01, ϕϕϕ p≤0.001; Mann-Whitney U test). The * are calculated respect to cisplatin or oxalilplatin, ϕ are calculated respect to vehicle.

Table S4. Enrichr analysis

KEGG 2021 Human

Index	Name	P-value	Adjusted p-value	Odds Ratio	Combined score
1	PI3K-Akt signaling pathway	0.00003672	0.008739	3.37	34.38
2	Small cell lung cancer	0.00008568	0.01020	6.25	58.49
3	Cellular senescence	0.0001528	0.01040	4.51	39.61
4	Kaposi sarcoma-associated herpesvirus infection	0.0002039	0.01040	3.98	33.85
5	Hippo signaling pathway	0.0002186	0.01040	4.30	36.24
6	Epstein-Barr virus infection	0.0003022	0.01143	3.79	30.75
7	Toxoplasmosis	0.0003361	0.01143	5.04	40.31
8	Hypertrophic cardiomyopathy	0.0004719	0.01404	5.51	42.22
9	TGF-beta signaling pathway	0.0006137	0.01623	5.26	38.89
10	Human cytomegalovirus infection	0.0007471	0.01778	3.38	24.35
11	Hepatitis B	0.0009161	0.01881	3.86	26.98
12	Amoebiasis	0.0009980	0.01881	4.81	33.26
13	Chronic myeloid leukemia	0.001106	0.01881	5.59	38.04
14	Pancreatic cancer	0.001106	0.01881	5.59	38.04
15	Pathways in cancer	0.001514	0.02403	2.33	15.12
16	Human immunodeficiency virus 1 infection	0.001680	0.02498	3.25	20.76
17	MAPK signaling pathway	0.002060	0.02861	2.80	17.32
18	Gastric cancer	0.002164	0.02861	3.71	22.76
19	Osteoclast differentiation	0.003495	0.04378	3.81	21.53
20	FoxO signaling pathway	0.004146	0.04531	3.68	20.20
21	Renal cell carcinoma	0.004159	0.04531	5.08	27.84
22	AGE-RAGE signaling pathway in diabetic complications	0.004446	0.04531	4.16	22.51
23	Proteoglycans in cancer	0.004531	0.04531	3.00	16.21
24	Melanoma	0.004989	0.04531	4.85	25.71
25	Non-small cell lung cancer	0.004989	0.04531	4.85	25.71
26	p53 signaling pathway	0.005290	0.04531	4.78	25.05
27	Rap1 signaling pathway	0.005293	0.04531	2.93	15.35
28	Human papillomavirus infection	0.005330	0.04531	2.47	12.93
29	Signaling pathways regulating pluripotency of stem cells	0.006653	0.05460	3.36	16.82
30	Human T-cell leukemia virus 1 infection	0.006910	0.05482	2.80	13.94
31	TNF signaling pathway	0.007667	0.05886	3.68	17.94

MSigDB Hallmark 2020

Index	Name	P-value	Adjusted p-value	Odds Ratio	Combined score
1	Epithelial Mesenchymal Transition	2.048e-9	9.216e-8	6.68	133.58
2	Estrogen Response Early	5.028e-7	0.00001131	5.42	78.56
3	Estrogen Response Late	0.000002742	0.00004112	5.01	64.18
4	TNF-alpha Signaling via NF-kB	0.00006471	0.0007280	4.22	40.71
5	Androgen Response	0.0008879	0.006983	4.92	34.55
6	Cholesterol Homeostasis	0.0009616	0.006983	5.75	39.96
7	p53 Pathway	0.001086	0.006983	3.46	23.59
8	UV Response Dn	0.001746	0.009824	3.85	24.43
9	IL-2/STAT5 Signaling	0.003733	0.01736	3.10	17.33
10	Hypoxia	0.003858	0.01736	3.08	17.14
11	TGF-beta Signaling	0.009429	0.03468	5.19	24.19
12	Mitotic Spindle	0.01199	0.03468	2.73	12.08
13	Apoptosis	0.01232	0.03468	2.96	13.02
14	Myogenesis	0.01233	0.03468	2.72	11.95
15	Interferon Gamma Response	0.01233	0.03468	2.72	11.95
16	Xenobiotic Metabolism	0.01233	0.03468	2.72	11.95

TF Perturbations Followed by Expression

Index	Name	P-value	Adjusted p-value	Odds Ratio	Combined score
1	NFKB1 ACTIVATION HUMAN GSE20736 CREEDSID GENE 2522 UP	1.746e-17	3.369e-14	8.85	341.61
2	EPAS1 KD HUVEC HUMAN GSE62974 RNASEQ UP	1.405e-12	1.356e-9	6.21	169.54
3	GTF2I KO MOUSE GSE48790 CREEDSID GENE 1451 DOWN	1.464e-11	9.420e-9	6.68	166.57
4	EGR3 KD HUMAN GSE52108 CREEDSID GENE 2233 DOWN	2.775e-11	1.339e-8	5.02	121.99
5	GTF2I KO MOUSE GSE48790 CREEDSID GENE 1452 DOWN	4.273e-11	1.649e-8	6.30	150.38
6	POU5F1 KD HUMAN GSE21135 CREEDSID GENE 1328 UP	1.359e-10	4.171e-8	4.99	113.47
7	ARID3A OE MOUSE GSE56853 CREEDSID GENE 1338 UP	1.623e-10	4.171e-8	5.35	120.60
8	FLI1 KD HUMAN GSE27524 CREEDSID GENE 1598 UP	1.729e-10	4.171e-8	4.77	107.17

Index	Name	P-value	Adjusted p-value	Odds Ratio	Combined score
9	SPDEF KD HUMAN GSE40985 CREEDSID GENE 2606 UP	2.069e-10	4.436e-8	5.28	117.81
10	GATA3 OE HUMAN GSE24249 CREEDSID GENE 649 UP	2.788e-10	4.892e-8	5.20	114.44
11	POU5F1 KD MOUSE GSE56853 CREEDSID GENE 1336 UP	2.788e-10	4.892e-8	5.20	114.44
12	ZNF207 OE HUMAN GSE9951 CREEDSID GENE 1581 DOWN	3.737e-10	6.011e-8	5.12	111.20
13	FLI1 KD HUMAN GSE27524 CREEDSID GENE 1599 UP	6.128e-10	8.045e-8	5.20	110.31
14	FLI1 KD HUMAN GSE27524 CREEDSID GENE 1604 UP	6.128e-10	8.045e-8	5.20	110.31
15	WT1 KO MOUSE GSE15325 CREEDSID GENE 2156 UP	6.253e-10	8.045e-8	4.99	105.68
16	DUX4 OE HUMAN GSE33799 CREEDSID GENE 1430 UP	1.098e-9	1.324e-7	5.51	113.71
17	ZNF589 SIRNA MDAMB231 HUMAN GSE79586 RNASEQ DOWN	2.240e-9	2.543e-7	5.55	110.60
18	ATF3 SIRNA HDF HUMAN GSE81405 RNASEQ DOWN	2.947e-9	3.160e-7	5.20	102.16
19	ARID3A OE MOUSE GSE56853 CREEDSID GENE 1339 UP	5.551e-9	5.639e-7	4.80	91.17
20	POU5F1 KD HUMAN GSE21135 CREEDSID GENE 1329 UP	7.938e-9	7.660e-7	4.35	81.20
21	STAT3 SIRNA MDAMB468 HUMAN GSE85579 RNASEQ UP	8.502e-9	7.814e-7	4.68	86.96
22	EZH2 SHRNA HUVEC HUMAN GSE71164 RNASEQ UP	9.859e-9	8.649e-7	5.63	103.83
23	IRX6 SIRNA MDAMB231 HUMAN GSE79586 RNASEQ DOWN	1.039e-8	8.722e-7	5.31	97.65
24	TBX3 SHRNA HFF HUMAN GSE76572 RNASEQ UP	1.161e-8	9.337e-7	4.60	83.98
25	ZEB1 OE CFPAC1 HUMAN GSE64558 RNASEQ DOWN	1.281e-8	9.887e-7	5.53	100.57
26	ETS1 SHRNA DU145 HUMAN GSE59020 RNASEQ UP	2.900e-8	0.000002152	4.20	72.85
27	FLI1 KD HUMAN GSE27524 CREEDSID GENE 1600 UP	3.444e-8	0.000002405	4.31	74.11
28	FLI1 KD HUMAN GSE27524 CREEDSID GENE 1607 UP	3.489e-8	0.000002405	4.68	80.41
29	PAX7 OE H9 HUMAN GSE98976 PROLIFMYOG RNASEQ UP	5.249e-8	0.000003493	4.21	70.51
30	PRRX1 SIRNA BT549 HUMAN GSE79586 RNASEQ DOWN	5.877e-8	0.000003750	4.99	83.07
31	FLI1 KD HUMAN GSE27524 CREEDSID GENE 1601 UP	6.023e-8	0.000003750	4.17	69.36

Index	Name	P-value	Adjusted p-value	Odds Ratio	Combined score
32	PHF20 SHRNA H1792 HUMAN GSE82115 RNASEQ UP	1.035e-7	0.000006239	8.30	133.56
33	ESR1 KD HUMAN GSE37820 CREEDSID GENE 2326 DOWN	1.565e-7	0.000009155	4.44	69.65
34	FLI1 KD HUMAN GSE27524 CREEDSID GENE 1597 UP	1.879e-7	0.00001052	4.20	65.12
35	NEUROG1 OE HUMAN GSE18296 CREEDSID GENE 1426 DOWN	1.907e-7	0.00001052	4.39	67.86
36	NR2F2 KD HUMAN GSE33182 CREEDSID GENE 822 UP	2.016e-7	0.00001081	4.82	74.38
37	MYC OE U2OS HUMAN GSE59819 RNASEQ UP	2.633e-7	0.00001337	5.33	80.78
38	MYC OE U2OS HUMAN GSE66789 RNASEQ UP	2.633e-7	0.00001337	5.33	80.78
39	HSF1 KD HUMAN GSE3697 CREEDSID GENE 782 UP	2.802e-7	0.00001387	5.31	80.04
40	PRRX1 SIRNA MDAMB231 HUMAN GSE79586 RNASEQ DOWN	3.144e-7	0.00001517	4.94	73.95
41	MYB KD HUMAN GSE49286 CREEDSID GENE 1842 DOWN	5.041e-7	0.00002373	4.29	62.26
42	HOXA11 SIRNA MDAMB231 HUMAN GSE79586 RNASEQ DOWN	5.710e-7	0.00002624	5.36	77.03
43	EGR3 KD HUMAN GSE52108 CREEDSID GENE 2231 DOWN	5.857e-7	0.00002629	4.06	58.32
44	ATF3 SIRNA HDF HUMAN GSE81405 RNASEQ UP	6.095e-7	0.00002674	4.45	63.64
45	SPDEF KD HUMAN GSE40985 CREEDSID GENE 2606 DOWN	7.263e-7	0.00003075	4.91	69.43
46	BNC2 SIRNA BT549 HUMAN GSE79586 RNASEQ DOWN	7.330e-7	0.00003075	5.25	74.09
47	GATA3 OE MDAMB231 HUMAN GSE72141 RNASEQ UP	7.557e-7	0.00003103	4.62	65.05
48	HIF1A OE 786O HUMAN GSE67237 RNASEQ UP	9.470e-7	0.00003808	3.93	54.53
49	PIN1 DEPLETION HUMAN GSE26262 CREEDSID GENE 477 UP	9.801e-7	0.00003857	4.52	62.57
50	ZFX KO MOUSE GSE7069 CREEDSID GENE 177 UP	0.000001012	0.00003857	4.08	56.39

Table S5. Clinical pathological data of iCCA patients (n=68)

	Mean	SD
Age	62,63	11,51
Tumor size	64,35	35,78
SEX		
F	29	
M	25	
Unknown	14	
Stage		
2	3	
3	8	
4a	12	
4b	22	
Background disease		
cirrhosis	2	
fibrisis w/o cirrhosis	1	
auto-immune hepatitis/Primary sclerosing cholangitis	1	
Perineural invasion		
Yes	17	
No	29	
ND	22	
Infiltration - potral tract		
Yes	11	
No	25	
ND	32	
Metastatic sites		
lymph nodes	10	
colon	3	
lung	3	
other	6	

Table S6. List of primers

Gene	Sequence
AFP-FW	AAGGCCAGGAACAGGAAGTC
AFP-REV	CACACCGAATGAAAGACTCG
EpCAM-FW	TGTGGTGATAGCAGTTGTTGC
EpCAM-REV	CTATGCATCTCACCCATCTCC
LGR5-FW	CTTCCAACCTCAGCGTCTTC
LGR5-REV	TTTCCCGCAAGACGTAACTC
CD13-FW	CAGTGACACGACGA TTCTCC
CD13-REV	CCTGTTTCCTCGTTGTCCTT
CD133-FW	GCTTCAGGAGTTTCA TGTTGG
CD133-REV	GGGGAATGCCTACATCTGG
NANOG-FW	GTCTCGTATTTGCTGCATCG
NANOG-REV	GAAACACTCGGTGAAATCAGG
BMI1-FW	TTGCTTTGGTCGAACTTGG
BMI1-REV	GTGCTTCTTTTGCAGACTGG
CMYC-FW	CGGAACTCTTGTGCGTAAGG
CMYC-REV	ACTCAGCCAAGGTTGTGAGG
KLF4-FW	AGACAGTCTGTTATGCACTGTGG
KLF4-REV	TGTTCTGCTTAAGGCATACTTGG
SOX-2-FW	ATGGGTTCGGTGGTCAAGT
SOX-2-REV	GGAGGAAGAGGTAACCACAGG
BMP4-FW	AGCGTAGCCCTAAGCATCAC
BMP4-REV	AGTCATTCCAGCCCACATCG
YAP-FW	ACCCTCGTTTTGCCATGAAC
YAP-REV	TTGTTTCAACCGCAGTCTCTC
STAT3-FW	GGCATTCGGGAAGTATTGTCG
STAT3-REV	GGTAGGCGCCTCAGTCGTATC
HNF4-FW	CTCGTCGACATGGACATGGCCGACTAC
HNF4-REV	GGCTTGCTAGATAACTTCCTGCTTGGT
ECAD-FW	AGGCCAAGCAGCAGTACATT
ECAD-REV	A TTCACA TCCAGCACA TCCA
VIM-FW	ACACCCTGCAATCTTTCAGACA
VIM-REV	GATTCCACTTTGCGTTCAAGGT
CTNNB1-FW	GCTGGGACCTTGCATAACCTT
CTNNB1-REV	ATTTTCACCAGGGCAGGAATG
ZEB1-FW	AAGAAAGTGTTACAGATGCAGCTG
ZEB1-REV	CCCTGGTAACACTGTCTGGTC
ZEB2-FW	AGGGACAGA TCAGCACCAAA
ZEB2-REV	GTGCGAACTGTAGGAACCAG
SNAIL-FW	CCTCCCTGTCAGATGAGGAC
SNAIL-REV	CAAGGAATACCTCAGCCTGG
SLUG-FW	ACAGCGAACTGGACACACAT
SLUG-REV	GATGGGGCTGTATGCTCCT
VEGFa-FW	CACTGAGGAGTCCAACATCAC
VEGFa-REV	AGGAAGCTCATCTCTCCTATGT
ABCF1-REV	CCCTTGTATTCATTGATGGC
ABCF1-FW	CTCATCTTGGACGAGCC
ABCC2-REV	GATAGCTGTCCGTACTTTTAC
ABCC2-FW	AAATTGCTGATCTCCTTTGC
ABCB1-REV	AGTCTGCATTCTGGATGG

ABCB1-FW	AGTGAAAAGGTTGTCCAAG
ABCG2-REV	GGCTTTCTACCTGCACGAAAACCAGTTGAG
ABCG2-FW	ATGGCGTTGAGACCAG

Table S7. List of antibodies

Antibody	Manufacturer	Dilution	Catalog number
Phospho AKT (Ser473)	Cell Signaling Technology	1:1000	#9271
AKT	Cell Signaling Technology	1:1000	#9272
Phospho STAT3 (Y705)	Cell Signaling Technology	1:1000	#9145
STAT3	Cell Signaling Technology	1:1000	#30835
Phospho ERK1/2 (Thr2020/Y204)	Cell Signaling Technology	1:1000	#9101
ERK1/2	Cell Signaling Technology	1:1000	#4348
Phospho P38 (Thr180/Y182)	Cell Signaling Technology	1:1000	#4511
P38	Abcam	1:1000	ab59461
cMYC	Cell Signaling Technology	1:1000	#5605
P27	Cell Signaling Technology	1:1000	#3686
P21	Cell Signaling Technology	1:1000	#2947
FASN	Cell Signaling Technology	1:1000	#3180
AceCS1	Cell Signaling Technology	1:1000	#3658
ACSL1	Cell Signaling Technology	1:1000	#9189
ACAC	Cell Signaling Technology	1:1000	#3666
ACLY	Cell Signaling Technology	1:1000	#4332
PPARγ	Cell Signaling Technology	1:1000	#2430
Phospho mTOR (Ser2448)	Cell Signaling Technology	1:1000	#2971
mTOR	Cell Signaling Technology	1:1000	#2983
Phospho S6K (Thr689)	Cell Signaling Technology	1:1000	#9205
S6K	Cell Signaling Technology	1:1000	#9202
β-actin	Sigma Aldrich	1:2500	A5441
Vinculin	Sigma Aldrich	1:2500	V9131

Raw data for western blotting

Fig.3 D

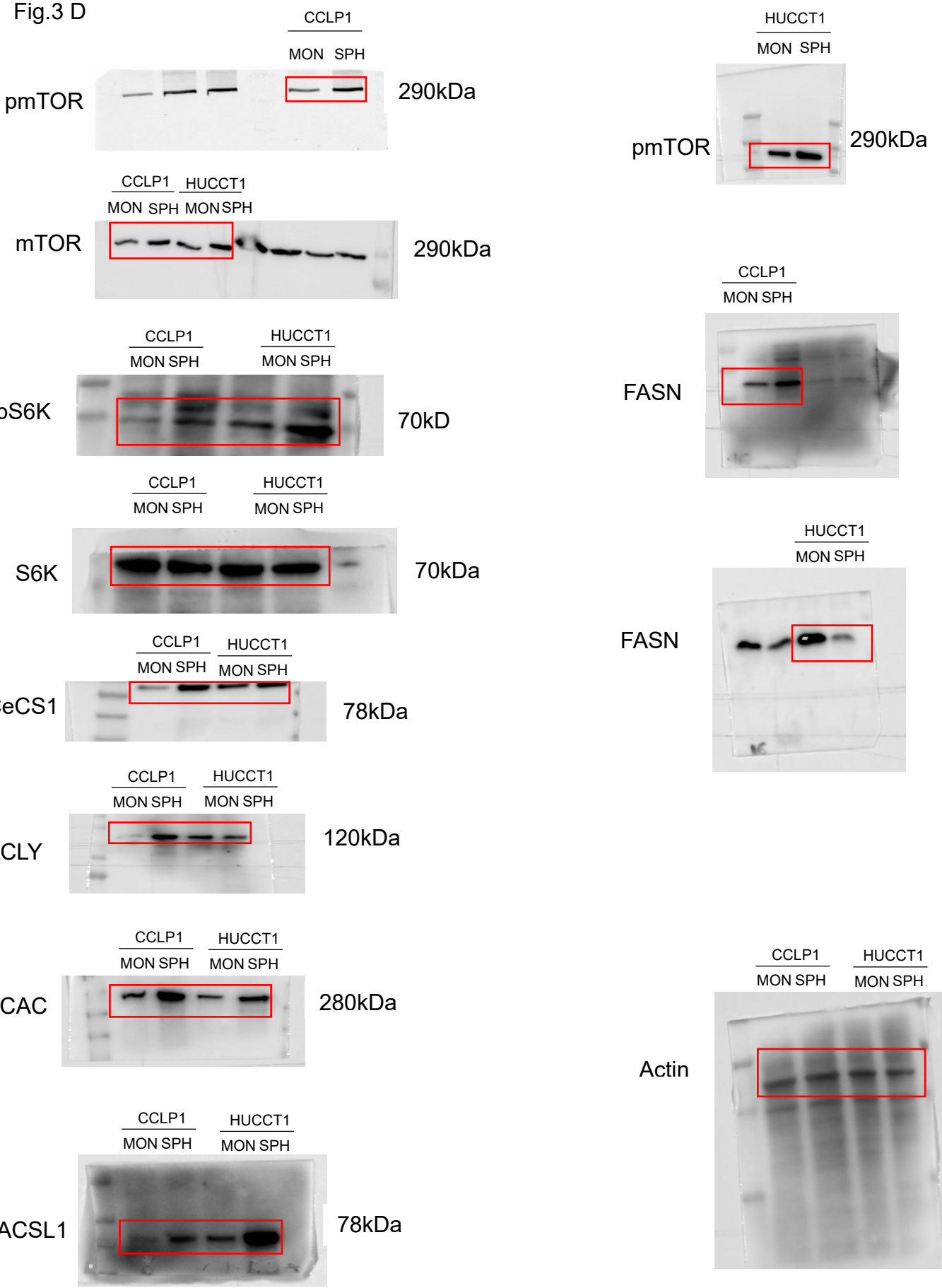

Fig.7 E

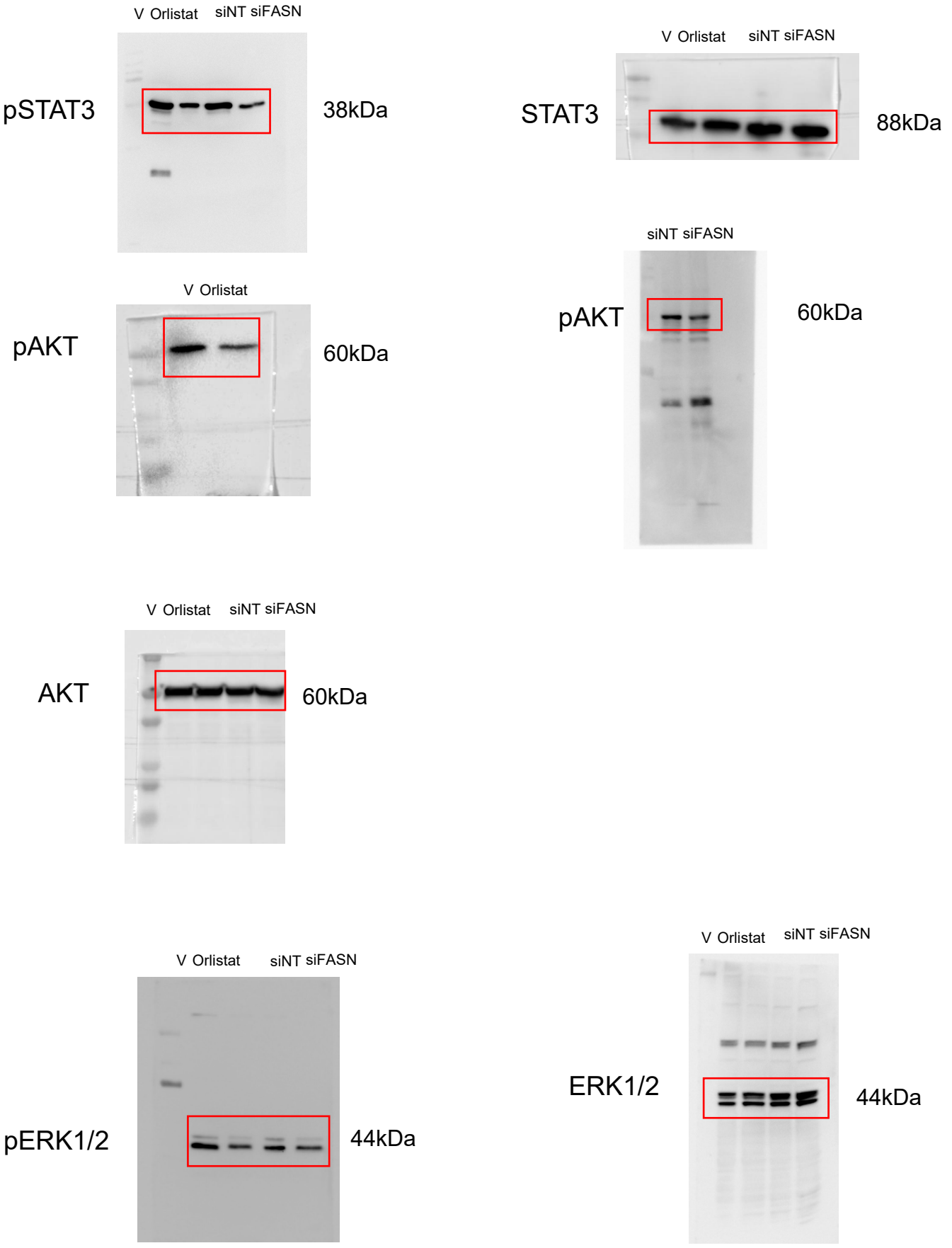
V Orlistat
siNT siFASN
pSTAT3
38kDa
V Orlistat
siNT siFASN
STAT3
88kDa
V Orlistat
pAKT
60kDa
siNT siFASN
pAKT
60kDa
V Orlistat
siNT siFASN
AKT
60kDa
V Orlistat
siNT siFASN
pERK1/2
44kDa
V Orlistat
siNT siFASN
ERK1/2
44kDa

Fig.7 E

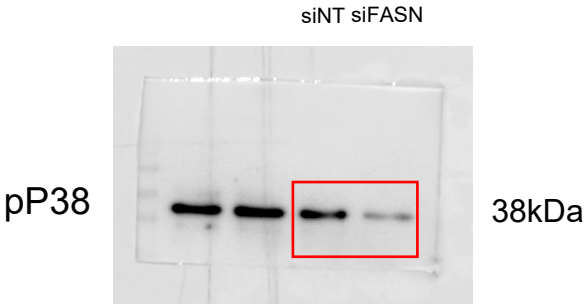
siNT siFASN
pP38
38kDa

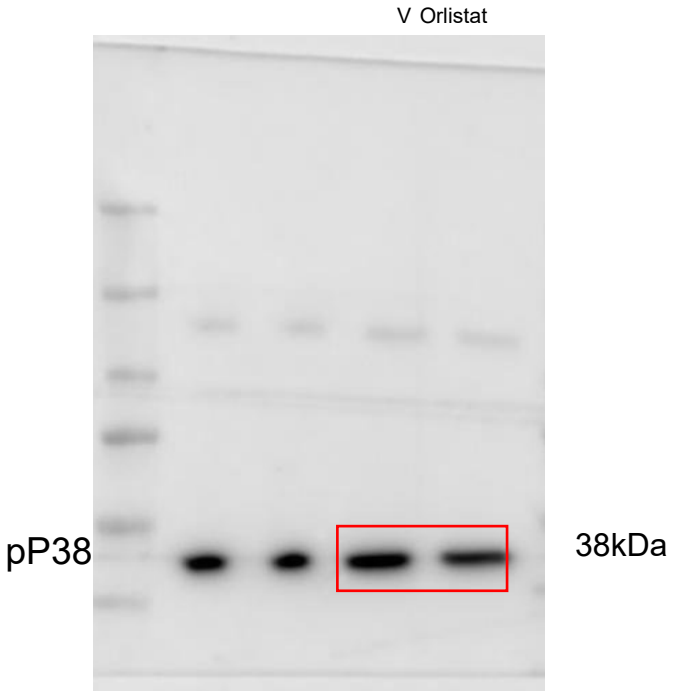
V Orlistat
pP38
38kDa

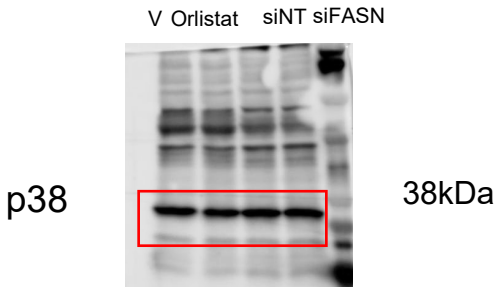
V Orlistat siNT siFASN
p38
38kDa

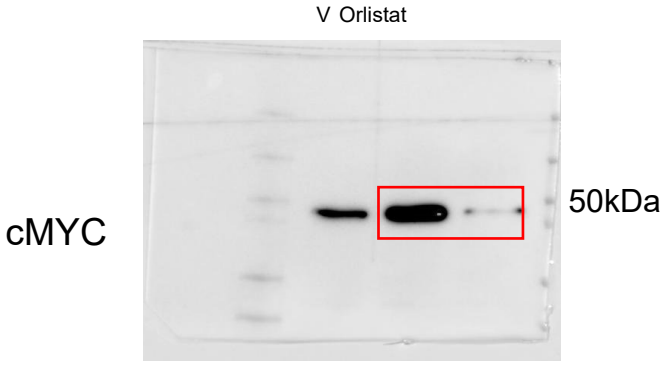
V Orlistat
cMYC
50kDa


siNT siFASN
cMYC
50kDa

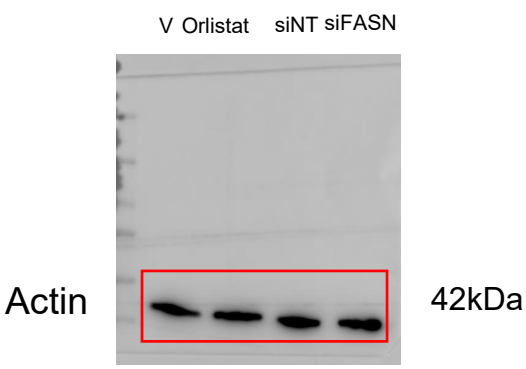
V Orlistat siNT siFASN
Actin
42kDa

Fig.8 F

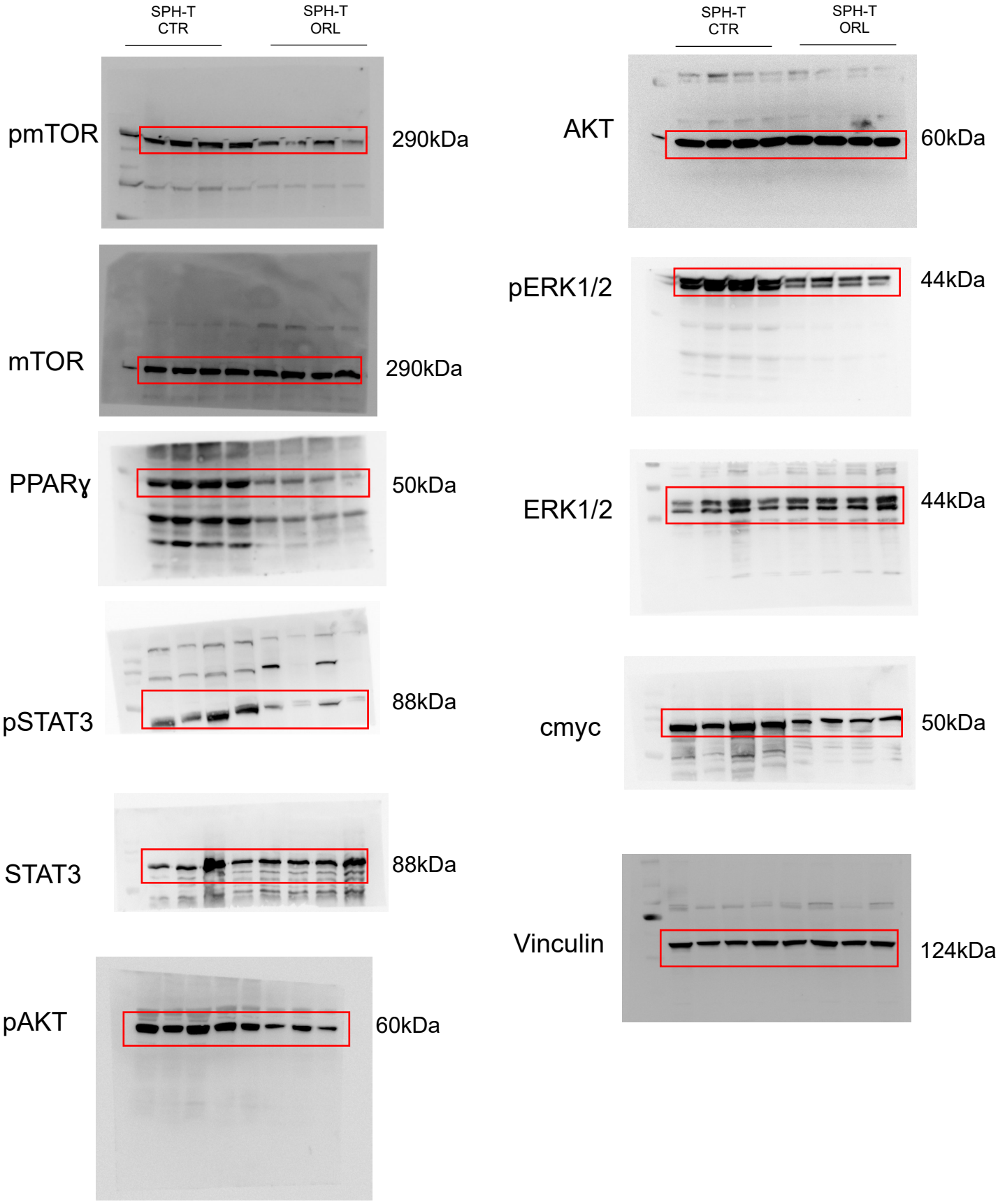
SPH-T CTR
SPH-T ORL
pmTOR
290kDa
mTOR
290kDa
PPARγ
50kDa
pSTAT3
88kDa
STAT3
88kDa
pAKT
60kDa
SPH-T CTR
SPH-T ORL
AKT
60kDa
pERK1/2
44kDa
ERK1/2
44kDa
cmyc
50kDa
Vinculin
124kDa

Fig.8 F

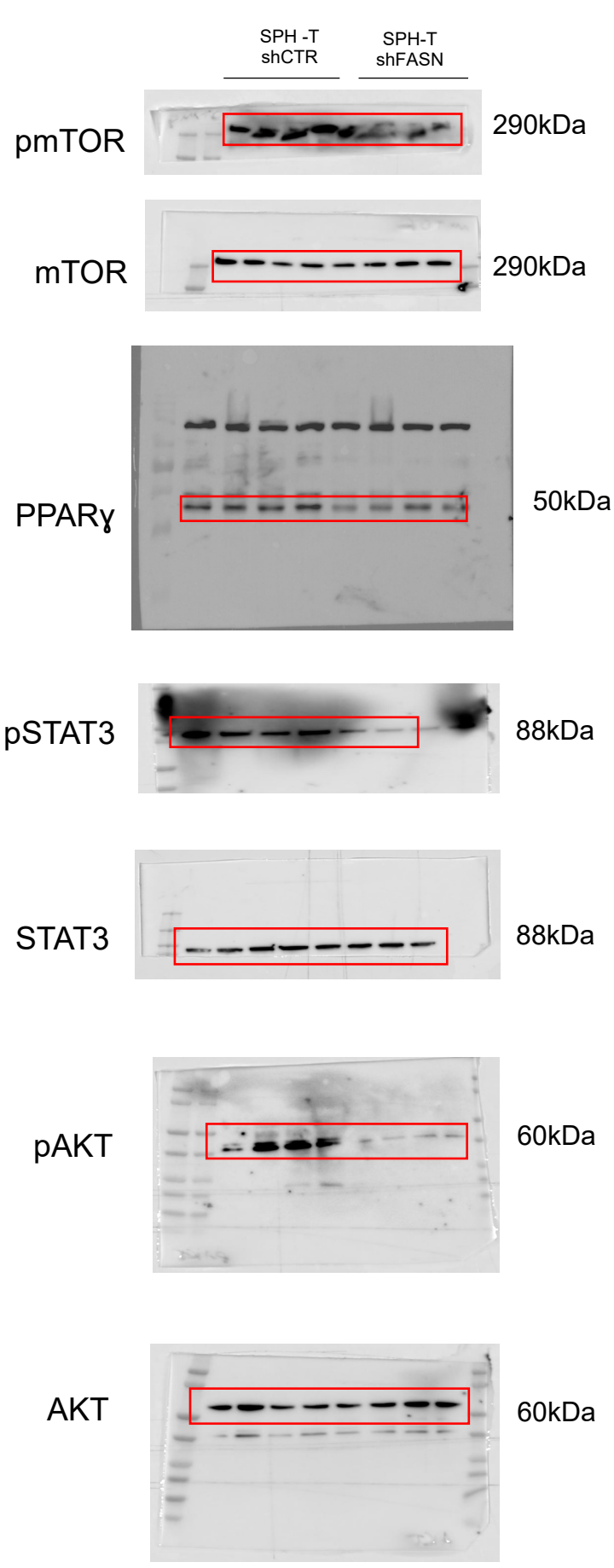
SPH -T shCTR
SPH-T shFASN
pmTOR
290kDa
mTOR
290kDa
PPARγ
50kDa
pSTAT3
88kDa
STAT3
88kDa
pAKT
60kDa
AKT
60kDa

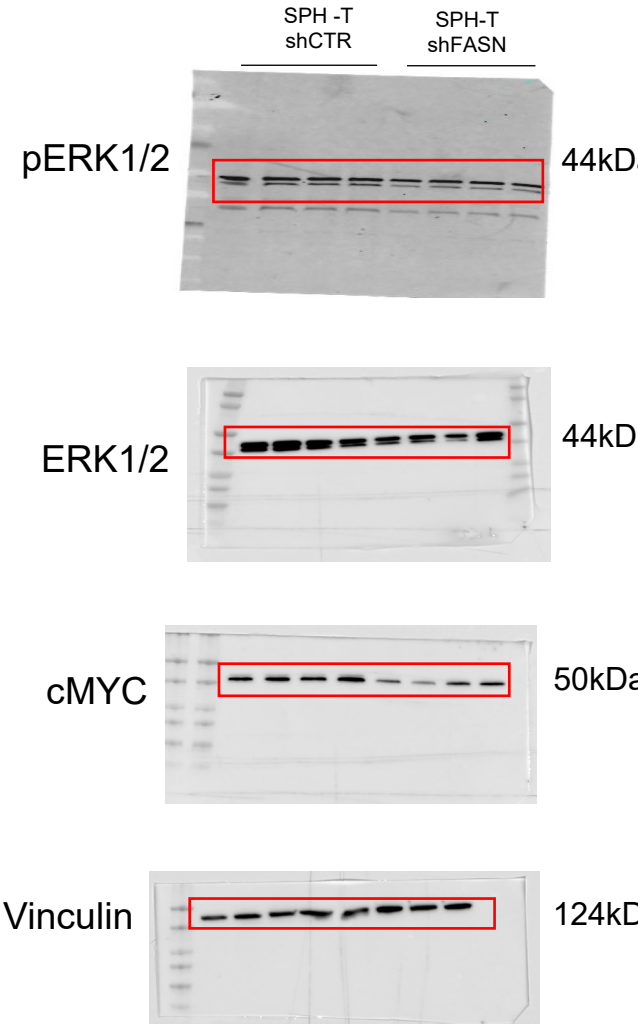
SPH -T shCTR
SPH-T shFASN
pERK1/2
44kD
ERK1/2
44kD
cMYC
50kDa
Vinculin
124kD

Supplementary references
Author names in bold designated shared co-first authorship

1. **Raggi C, Correnti M,** Sica A, et al. Cholangiocarcinoma stem-like subset shapes tumor-initiating niche by educating associated macrophages. J Hepatol 2017;66:102-115.
2. Raggi C, Taddei ML, Sacco E, et al. Mitochondrial oxidative metabolism contributes to a cancer stem cell phenotype in cholangiocarcinoma. J Hepatol 2021;74:1373-1385.
3. Masoodi M, Gastaldelli A, Hyotylainen T, et al. Metabolomics and lipidomics in NAFLD: biomarkers and non-invasive diagnostic tests. Nat Rev Gastroenterol Hepatol 2021;18:835-856.
4. Andersen JB, Spee B, Blechacz BR, et al. Genomic and genetic characterization of cholangiocarcinoma identifies therapeutic targets for tyrosine kinase inhibitors. Gastroenterology 2012;142:1021-1031.e1015.
5. Chen S, Zhou Y, Chen Y, et al. fastp: an ultra-fast all-in-one FASTQ preprocessor. Bioinformatics 2018;34:i884-i890.
6. Patro R, Duggal G, Love MI, et al. Salmon provides fast and bias-aware quantification of transcript expression. Nat Methods 2017;14:417-419.
7. Soneson C, Love MI, Robinson MD. Differential analyses for RNA-seq: transcript-level estimates improve gene-level inferences. F1000Res 2015;4:1521.
8. Smedley D, Haider S, Ballester B, at al. BioMart--biological queries made easy. BMC Genomics 2009;10:22.
9. **Subramanian A, Tamayo P**, Mootha VK, et al. Gene set enrichment analysis: a knowledge-based approach for interpreting genome-wide expression profiles. Proc Natl Acad Sci U S A 2005;102:15545-15550.
10. Mootha VK, Lindgren CM, Eriksson KF, et al. PGC-1alpha-responsive genes involved in oxidative phosphorylation are coordinately downregulated in human diabetes. Nat Genet 2003;34:267-273.
11. Liberzon A, Subramanian A, Pinchback R, et al. Molecular signatures database (MSigDB) 3.0. Bioinformatics 2011;27:1739-1740
12. Liberzon A, Birger C, Thorvaldsdóttir H, et al. The Molecular Signatures Database (MSigDB) hallmark gene set collection. Cell Syst 2015;1:417-425.